buildings

MDPI

Article

Dynamic Behavior of Lighting GFRP Pole Under Impact Loading

Mahmoud T. Nawar [1,2], Ahmed Elbelbisi [2,3,*], Mostafa E. Kaka [2], Osama Elhosseiny [2] and Ibrahim T. Arafa [2]

[1] Engineering Management Department, College of Engineering, Prince Sultan University, Riyadh 11586, Saudi Arabia; mnawar@psu.edu.sa
[2] Structural Engineering Department, Zagazig University, Zagazig 44519, Egypt; mekaka@zu.edu.eg (M.E.K.); dr.ossama@bect.net (O.E.); ibrahimtalaat@zu.edu.eg (I.T.A.)
[3] Civil and Environmental Engineering, University of Missouri, Columbia, MO 65211, USA
* Correspondence: aelbelbisi@missouri.edu

Abstract

Vehicle collisions with street lighting poles generate extremely high impact forces, often resulting in serious injuries or fatalities. Therefore, enhancing the structural resilience of pole bases is a critical engineering objective. This study investigates a comprehensive dynamic analysis conducted with respect to base material behavior and energy absorption of GFRP lighting pole structures under impact loads. A finite element (FE) model of a 5 m-tall tapered GFRP pole with a steel base sleeve, base plate, and anchor bolts was developed. A 500 kg drop-weight impact at 400 mm above the base simulated vehicle collision conditions. The model was validated against experimental data, accurately reproducing the observed failure mode and peak force within 6%. Parametric analyses explored variations in pole diameter, wall thickness, base plate size and thickness, sleeve height, and anchor configuration. Results revealed that geometric parameters—particularly wall thickness and base plate dimensions—had the most significant influence on energy absorption. Doubling the wall thickness reduced normalized energy absorption by approximately 76%, while increases in base plate size and thickness reduced it by 35% and 26%, respectively. Material strength and anchor bolt configuration showed minimal impact. These findings underscore the importance of optimizing pole geometry to enhance crashworthiness. Controlled structural deformation improves energy dissipation, making geometry-focused design strategies more effective than simply increasing material strength. This work provides a foundation for designing safer roadside poles and highlights areas for further exploration in base configurations and connection systems.

Keywords: GFRP; street poles; dynamic analysis; impact test; anchor bolt; toughness; ABAQUS

Academic Editor: Eric M. Lui

Received: 19 May 2025
Revised: 29 June 2025
Accepted: 1 July 2025
Published: 3 July 2025

Citation: Nawar, M.T.; Elbelbisi, A.; Kaka, M.E.; Elhosseiny, O.; Arafa, I.T. Dynamic Behavior of Lighting GFRP Pole Under Impact Loading. *Buildings* **2025**, *15*, 2341. https://doi.org/10.3390/buildings15132341

1. Introduction

The rising incidence of vehicles colliding with roadside lighting poles could lead to thousands of individuals experiencing severe injuries, enduring permanent disabilities, or even losing their lives. To reduce the accidental effect on passengers, it is essential to implement measures that absorb the energy generated during such collisions [1]. This energy cannot be efficiently absorbed by the traditional lightening poles made of steel or wood [2–9]. Currently, centrifugally manufactured GFRP (Glass Fiber Reinforced Polymer) pipes are extensively employed as lighting and low-power transmission poles. This is primarily due to their exceptional strength-to-weight ratio, high electrical insulation

properties, cost-effectiveness, remarkable flexibility, and resistance to corrosion. The suggested new material exhibits impact characteristics that can slow down a vehicle and effectively soak up significant energy during collisions [10–12]. In order to improve the manufacturing process and refine pole design, we performed lateral loading experiments on 22 full-scale prototypes of fiber-reinforced polymer (FRP) poles through mechanical bending tests [13,14]. J. K. Son and A. Fam [15] explored the flexural characteristics of hollow FRP tubes and concrete-filled FRP tubes in their study, aiming to determine the optimal level of concrete filling for the optimization of FRP monopoles. Numerous studies have been conducted to analyze the static characteristics and long-term durability of these poles, resulting in enhancements in their anticipated dynamic performance [16,17]. Toughness is a key attribute for describing the poles because it plays a critical role in their capacity to absorb collision energy before breaking. Desai et al. [18] investigated the bending and buckling behavior of FRP poles and explored how the orientation of fibers influences the critical load [19,20]. Urgessa and Mohamadi [21] conducted a parametric study using finite element analysis to examine factors such as geometric characteristics, fiber alignment, the number of layers, and lamina thickness in FRP composite poles. Masmoudi et al. [14] explored the circumferential angles of fiber orientation in tapered filament welded GFRP poles through a combination of experimental tests and finite element models. A 3D finite element analysis of cantilevered (GFRP) tubular poles under lateral and axial loads revealed a significant influence of the GFRP laminate structure on the axial and flexural strengths of the poles [22]. In a finite element analysis conducted by H. Gao et al. [23] on GFRP poles, they discovered economic advantages and an innovative installation method for these poles. Furthermore, they confirmed that the pole's base exhibits adequate flexural bearing capacity, overturning stability, and durability. Awad et al. [24] conducted an experimental research program that involved five full-scale GFRP poles. The primary objectives were to determine the most efficient strengthening technique and to evaluate the impact of openings for connectors near the base. The results were compared to earlier research findings. In a separate study, Nawar et al. [25] investigated the effects of incorporating a steel sleeve at the base on the resilience of GFRP lighting poles. Their investigation utilized a combination of experimental and numerical analyses. Additionally, they reinforced the handle door to address any weaknesses near this area of the GFRP pole. Quasi-static experiments were conducted to establish a precise representation of static resistance. Consequently, the static resistance of the structural system plays a crucial role in practical engineering for predicting the dynamic response of structures. Moreover, the dynamic buckling was sensitive to the poles' boundary conditions. Especially, the local buckling of poles tends to occur close to the pole base [26]. The jointed composite GFRP poles were subjected to a combination of experimental surveys and finite element analyses, highlighting that the primary mode of failure near the base was local buckling. These findings indicated that to maintain the structural integrity of the joint, the minimum joint length should be at least 1/10 of the pole's total length, whether under static or dynamic conditions [27]. In a separate study, researchers employed experimental testing to determine the dynamic characteristics of aluminum light poles and assess the performance of a damping device in mitigating the effects of wind and winter storms [28]. The installation of an aluminum foam protective device had a notable impact on human safety during vehicle collisions with bridge columns, resulting in a 37.5% reduction in the peak impact force [29]. Moreover, H. Al-Thairy and Y.C. Wang [30] utilized the commercial finite element software ABAQUS/Explicit to forecast the vehicles' equivalent linear stiffness and developed simulations to replicate their head-on collisions with steel columns across a range of scenarios, encompassing varying impact speeds, axial load ratios, boundary conditions, and slenderness ratios. A. Elmarakbi and K. Sennah [3] performed a numerical analysis of the FRP

pole-soil system and found that the sandy soil has a highly resistance of pole movement at ground level than clayey soil. H. Kang and J. Kim [31] studied the damage analysis of steel column-footing connection subjected caused by the car impact. It was observed that reducing the pedestal height, increasing the pedestal area, and applying steel plate jacketing to the pedestal were effective in preventing damage. While extensive research has been conducted on the development of GFRP poles, the majority of these studies have concentrated on embedded poles, overlooking investigations into the pole base.

Consequently, there is a gap that needs addressing to improve the durability of GFRP poles and reinforce their ability to withstand vehicular collisions. Most available studies either neglect the base region or are limited to quasi-static testing conditions, leaving a notable gap in understanding how base geometry and structural detailing influence crash behavior. This study aims to fill this void by analyzing the dynamic characteristics of a simplified impact scenario, assessing the efficacy of utilizing GFRP lighting poles equipped with steel base sleeves. Additionally, it aims to anticipate the extent of vehicular damage in the vicinity of the pole base. This damage mitigation requires a certain level of flexibility to absorb the impact energy. Parametric studies are developed using a finite element model (FEM) to find out the most important factors affecting its toughness under impact load to improve its ability to dissipate the collision energy when cars collide with it to reduce the duration of the crushed car and occupant injuries.

2. Finite Element Analysis

The Finite Element (FE) method provides a cost-efficient substitute for expensive experiments. This method enables the investigation of a diverse range of parameters. In this research, we constructed three-dimensional nonlinear finite element models (FEM) using ABAQUS explicit V6.14 software.

These models included essential elements such as nodes, elements, material properties, dimensions, boundary constraints, and applied loads, presenting a streamlined analytical approach.

2.1. Validation Model

The accuracy of the Finite Element Analysis (FEA) modeling approach was confirmed through experimental trials conducted by Jun Wang and their research team [32]. Their experiments involved assessing the impact behavior of ten GFRP hollow and concrete-filled tubes using both a vertical drop weight test and a horizontal trolley traction impact test apparatus, as illustrated in Figure 1. The validation process specifically focused on a sample identified as IH4-1. IH4-1 represents a circular hollow GFRP tube made from E-Glass, featuring a longitudinal-circumferential fiber volume ratio of 4:1. The specimen had dimensions of 142 mm in diameter, 1050 mm in height, and a wall thickness of 5 mm.

The end of the tested tube was firmly fixed using a rigid steel abutment, and a 230 kg mass hammer was applied from a height of 0.5 m, 600 mm away from the fixed end of the tube.

For modeling the pole, fully integrated shell elements were utilized. In the case of the GFRP tube, a shell element (S4R) was used with a reduced integration algorithm. The impact drop hammer, made of high-strength steel, was modeled as a rigid object with a mass of 230 kg and a modulus of 201 GPa. The mechanical properties of the tested FRP tube were derived from the experimental testing performed by Jun Wang et al. [32] on specimen IH4-1, with a longitudinal tensile strength of 465 MPa, a longitudinal tensile modulus of 28 GPa, and a transverse tensile strength of 75 MPa. Figure 2 illustrates the Finite Element configuration for the drop weight impact test of the GFRP hollow tube. The rigid steel abutment, fixed at one end of the tube, was modeled as a fixed boundary condition, while

the other end remained free. The steel drop hammer was constrained from translation in all directions, except in the vertical direction (Y), to simulate the experimental conditions.

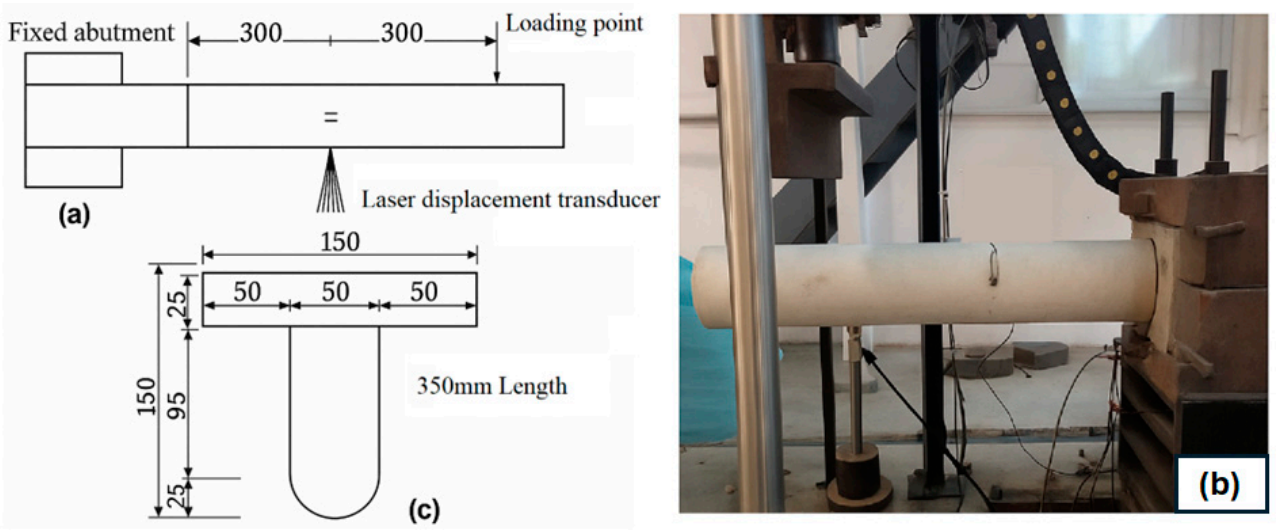

Figure 1. Impact testing by Jun Wang et al. [32]: (**a**) schematic of test setup, (**b**) test setup, and (**c**) drop hammer head.

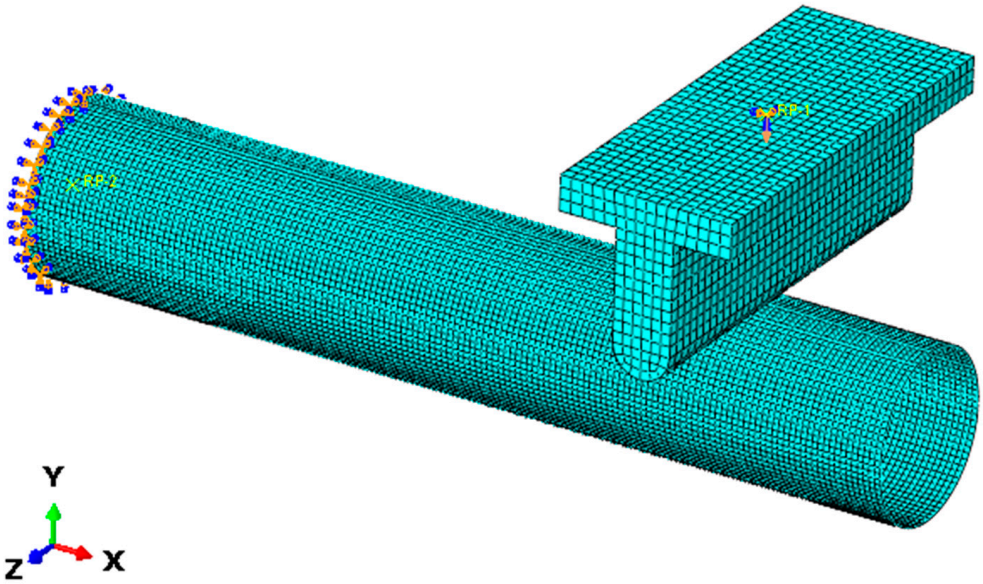

Figure 2. FE model configuration.

A mesh with a 10 mm size was used for the GFRP tube, and the size of the hammer head was adjusted to 20 mm in order to satisfy convergence criteria.

The interaction between the steel hammerhead and the surface of the GFRP tube was simulated using the surface-to-surface contact method. The simulation incorporated a penalty friction method with a friction coefficient of 0.25 to model the normal and tangential characteristics of surface-to-surface contact. Additionally, post-contact separation was considered in the analysis.

The impact load was applied by free-falling vertically from a 500 mm drop height. The technique that was used to model the impact load defined as the mass of the rigid hammer in the ABAQUS property module as the point Mass/Inertia of 230 kg. The velocity of the fall hammer just before hitting the GFRP pole surface was calculated from the general

dynamics equations and modeled as initial step conditions of the rigid hammer in the ABAQUS load module as predefined field velocity v2.

2.2. Validation Results

In order to establish the credibility of the developed FE model in emulating the GFRP tube's dynamic reaction under impact conditions, the numerical simulation outcomes were contrasted with experimental results.

In order to achieve accurate results within a reasonable computational timeframe, a mesh sensitivity analysis was carried out with three different element sizes: 5 mm, 10 mm, and 20 mm. The FE validations showcased reasonable projections of the impact load and displacement over time, as depicted in Figure 3. Moreover, both the numerical and experimental evaluations unveiled identical modes of failure, specifically, localized buckling and compression at the loading zone and the anchored end. The peak impact load anticipated by the FE model generally exceeded the experimental value by around 5.6%, while the maximum displacement was roughly 9.4% higher than the experimental value. These results highlight a strong agreement between the FE simulations and the outcomes from experiments. As a result, the validated FE model was utilized for additional investigations, delving into the impact of different factors on the overall structural response of the GFRP pole.

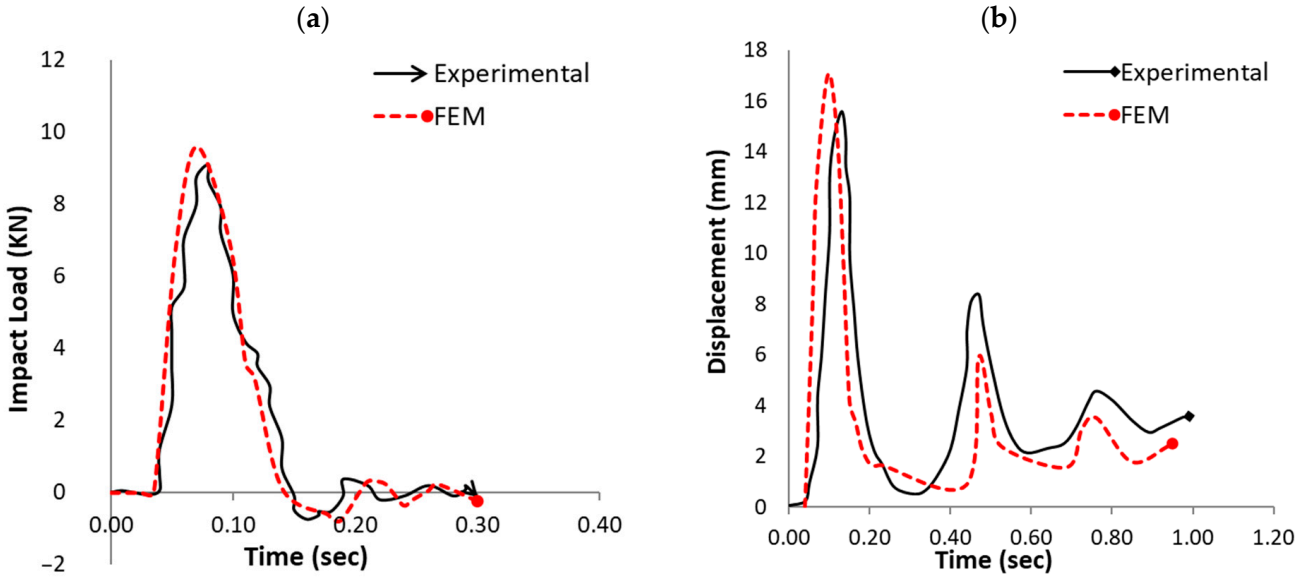

Figure 3. A comparison between the experimental and FE models for specimen (IH4-1): (**a**) impact load time history and (**b**) displacement time history.

2.3. Parametric Studies

For our investigation, we utilized the ABAQUS explicit V6.14 software to create a three-dimensional nonlinear finite element model (FEM) for simulating the dynamic behavior of the GFRP lighting pole. This FEM was based on the previously validated FE model.

The study was conducted on the first 1.5 m from the GFRP pole with base plate and anchor bolts base system to save computer time and because most of the cars hit this region when crashing into lighting poles. The same drop hammer shape and technique of the verified model were used to construct the model of the dynamic behavior of the GFRP pole under impact load, but the mass of the drop hammer was taken to be 500 kg, somewhat like a passenger car mass. The impact load acting at 400 mm from the base plate to simulate the impact height occurs in most passenger vehicles bumper heights.

2.3.1. FE Models Geometry

Flexible three-dimensional volumetric elements were utilized to model the concrete foundation, anchor bolts, base plate, steel sleeve, and GFRP pole. The falling steel hammer was represented as a rigid body, based on a validated design. The tapered geometry of the poles and steel sleeve was generated through a process of rotation and extrusion, incorporating variable diameters at the ends. Circular openings were included in the concrete foundation and base plate to represent the four anchor bolt holes and the electric cable entry hole, respectively. Each anchor was composed of a bolt shank, nut, and washer. The influence of these components on the dynamic response of the GFRP pole was accounted for in the analysis.

2.3.2. Element Types, Meshing, and Material Properties

The base plate, hammer, and concrete foundation were simulated using eight-node linear brick elements (C3D8R) with reduced integration. In contrast, the conical GFRP pole, steel sleeve, and epoxy resin were modeled using eight-node quadrilateral solid elements (Q8) employing the same reduced integration technique. This element type was selected for its ability to represent curved boundaries, allowing for an accurate evaluation of the epoxy resin layer's effect between the steel sleeve and the GFRP pole. Figure 4 presents the schematic of the impact load test and the finite element model configuration.

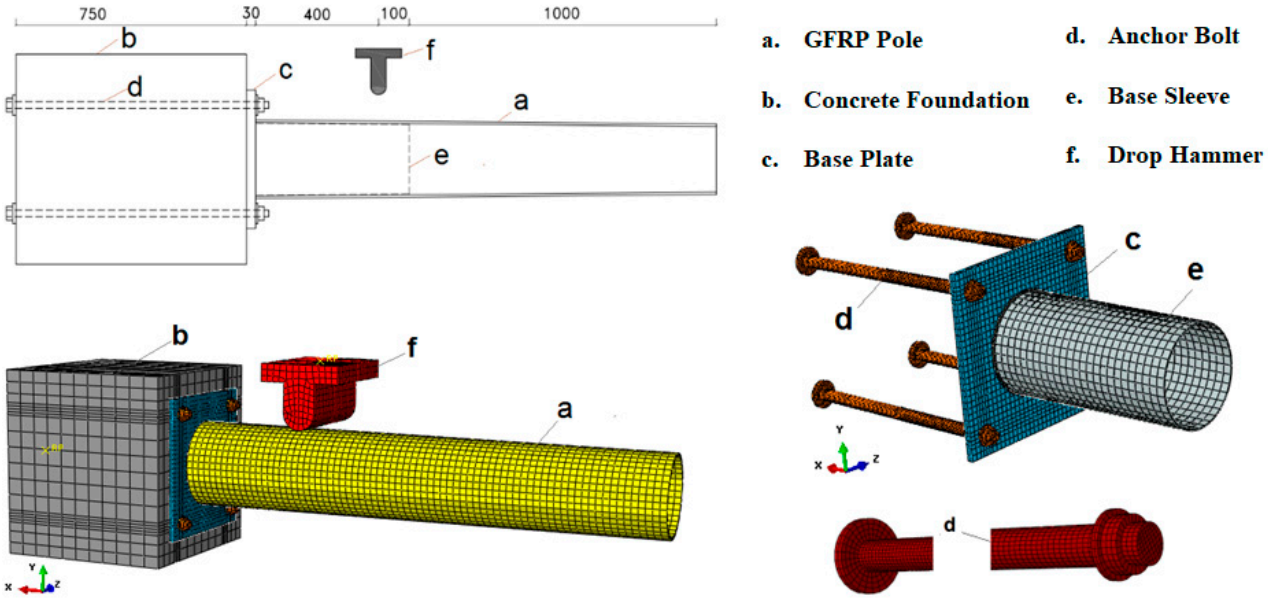

Figure 4. Finite element model schematic and configuration.

The various components of the finite element model were meshed independently. To satisfy the convergence criteria, a mesh size of 10 mm was applied to the GFRP pole, base plate, steel sleeve, and anchor bolts. In contrast, a coarser mesh of 20 mm was used for the falling hammer and the concrete foundation. Additionally, mesh refinement was introduced around the apertures for the four anchor bolts and the cable entry holes to ensure accuracy in these critical regions. The bi-linear relationships were used to model the stress–strain relationship of steel reinforcement. The modulus of elasticity and yielding stress were used to define the linear elastic part. Otherwise, the ultimate stress and plastic strain were used to define the strain hardening part. On the other hand, a linear relationship was adopted in this study to model the stress–strain relationship of GFRP. The equivalent modulus of elasticity and ultimate stress were used to define this relationship.

Table 1 summarizes the mechanical properties of the constituent materials used in fabricating the GFRP pole, including E-glass fibers and number 90 isophthalic polyester resin, as well as the resulting equivalent GFRP composite. These properties include density, Poisson's ratio, tensile and shear moduli, tensile strength, and the percentage of glass fiber by weight.

Table 1. Mechanical properties of e-glass fibers and number 90 isophthalic polyester resin.

Properties	E-Glass	# 90 Isophthalic Polyester Resin	Equivalent GFRP
Density (gm/cm^3)	2.54	1.08	1.85
Poisson's ratio (v)	0.2	0.3	0.25
Tensile modulus (GPa)	72	3.4	18
Shear modulus (Gpa)	30	1.37	4.8
Tensile strength (Mpa)	1500	79	370
Flexural strength (Mpa)	--	--	365
Percent of glass fiber by weight	--	--	45%

Table 2 lists the mechanical properties of the steel components used in the model, specifically the base sleeve, base plate, and anchor bolts. The properties include density, Poisson's ratio, tensile and shear moduli, tensile strength, and yield strength. These values were essential for accurately simulating the structural response under impact loading conditions.

Table 2. Mechanical properties of steel parts.

Material	Base Sleeve, Base Plate	Anchor Bolt
Density (gm/cm^3)	7.8	7.8
Poisson's ratio (v)	0.26	0.26
Tensile modulus (Gpa)	207	207
Shear Modulus (Gpa)	80	80
Tensile Strength (Mpa)	360	520
Yield Strength (Mpa)	240	360

2.3.3. Interaction Properties

All elements in the finite element model were connected using appropriate interaction definitions. Tie constraints were applied to ensure uniform load distribution across the full cross-section, linking reference points to the section surface via a rigid body tie method. To simulate the interaction between the epoxy resin and the conical surfaces of both the inner steel sleeve and the outer GFRP pole, a master–slave surface contact approach was used. Additionally, surface-to-surface contact was defined for interactions between various components, including the bolt head and washer, bolt shank and base plate holes, washer and base plate, base plate and foundation, and hammer head and GFRP pole. The tangential and normal behaviors of these contacts were governed by a penalty friction formulation, with a friction coefficient of 0.2. Further tie constraints were assigned to connect each base sleeve to the base plate, and to fix the anchor bolt shanks to the concrete foundation.

2.3.4. Loading and Boundary Conditions

The impact force was simulated by modeling a drop hammer with a mass of 500 kg, released from a height of 1.5 m and striking the system at a point located 400 mm from the

edge of the pole's base plate. To allow limited bending at the base plate, fixed constraints were applied to the nodes on the outer surfaces of the concrete foundation. These boundary conditions accounted for both the footing–ground interaction and the flexibility of the base plate. Translational and rotational movements of the foundation were restricted in the X, Y, and Z directions, while the hammer head was constrained to move only along the *Y*-axis, which aligned with the longitudinal direction of the GFRP pole. The reactions resulting from these boundary conditions were used to derive the impact load and displacement–time history curves for the analyzed GFRP poles.

3. FE Analysis and Discussions

The investigated parameters included key physical and material attributes: GFRP pole diameter (PD), wall thickness (PT), base plate dimensions (length BPL and breadth BPB), base plate thickness (BPT), electric cable hole diameter (HD), base plate steel grade (BPSG), base sleeve height (SH), sleeve thickness (ST), sleeve steel grade (SSG), number of anchor bolts (AN), anchor bolt diameter (AD), anchor bolt steel grade (ASG), and washer diameter (WD) (refer to Figure 5). The GFRP pole length was kept constant at 1.5 m across all simulations. Each pole configuration was labeled using a unique identifier in the format "parameter name—parameter value" to clearly track geometric changes and their corresponding peak impact force. For each case, the impact load–time history and peak impact force were obtained to evaluate the energy absorption capacity and impact resilience of the GFRP poles. Furthermore, Toughness is calculated by integrating the area under the load-deflection curve to express to improve its ability to dissipate the collision energy when cars collide with it.

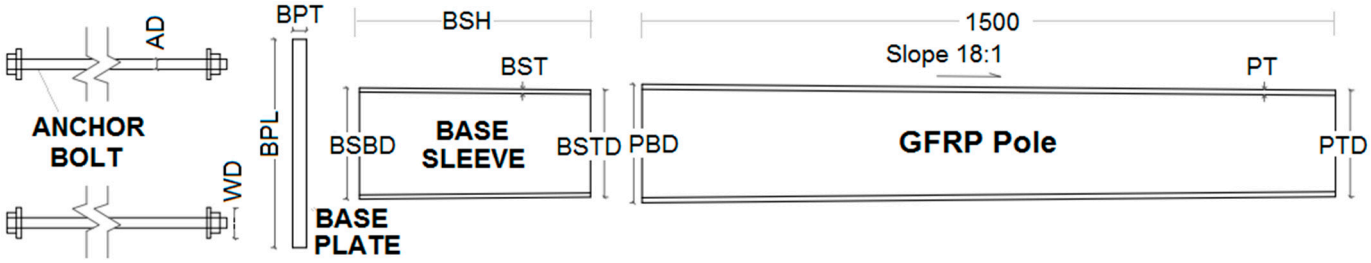

Figure 5. The geometric parameters of the study cases.

A dynamic analysis was conducted to determine the optimal properties for enhancing the performance of GFRP lighting pole bases under impact loads. The objective was to investigate methods to improve the dynamic response of these poles when subjected to vehicular impact, aiming to dissipate impact energy and reduce collision duration, thereby minimizing severe injuries and protecting passenger lives. A key indicator of improved passenger safety was the correlation between impact force and the displacement of the GFRP pole, particularly in scenarios involving early failure with limited toughness. Parametric sensitivity analyses were performed to examine the influence of various parameters on the dynamic response of the GFRP pole and the resulting peak impact force. A summary of the geometric properties and peak impact forces of the GFRP poles is presented in Table 3.

Table 3. A summary of the geometric properties and peak impact force of the GFRP poles.

Case Study	FE Pole	GFRP Pole Dimensions			Base Sleeve Dimensions					Base Plate Dimensions				Anchor bolts				Peak Impact Force (KN)
	Label	PBD	PTD	PT	BSSG	BSBD	BSTD	BST	BSH	BPSG	BPHD	BPT	BPL	ASG	WD	AD	AL	AN	
		(mm)	(mm)	(mm)		(mm)	(mm)	(mm)	(mm)		(mm)	(mm)	(mm)		(mm)	(mm)	(mm)		
GFRP Pole Thickness	PT6	256	229	**6**	S235	246	240	3	300	S235	0	30	450	S235	50	22	800	4	215
	PT8	256	229	**8**	S235	246	240	3	300	S235	0	30	450	S235	50	22	800	4	225
	PT10	256	229	**10**	S235	246	240	3	300	S235	0	30	450	S235	50	22	800	4	238
	PT12	256	229	**12**	S235	246	240	3	300	S235	0	30	450	S235	50	22	800	4	252
GFRP Pole Bottom Diameter	PBD184	**184**	**157**	8	S235	174	169	3	300	S235	0	30	450	S235	50	22	800	4	172
	PBD256	**256**	**229**	8	S235	246	277	3	300	S235	0	30	450	S235	50	22	800	4	223
	PBD328	**328**	**301**	8	S235	318	313	3	300	S235	0	30	450	S235	50	22	800	4	246
Base Plate Dimensions L, B	BPL450	256	229	8	S235	246	237	3	500	S235	0	15	**450**	S235	50	22	800	4	178
	BPL500	256	229	8	S235	246	237	3	500	S235	0	15	**500**	S235	50	22	800	4	189
	BPL550	256	229	8	S235	246	237	3	500	S235	0	15	**550**	S235	50	22	800	4	198
	BPL600	256	229	8	S235	246	237	3	500	S235	0	15	**600**	S235	50	22	800	4	248
Base Plate Thickness T	BPT10	256	229	8	S235	246	237	3	500	S235	0	**10**	450	S235	50	22	800	4	242
	BPT15	256	229	8	S235	246	237	3	500	S235	0	**15**	450	S235	50	22	800	4	255
	BPT20	256	229	8	S235	246	237	3	500	S235	0	**20**	450	S235	50	22	800	4	327
	BPT30	256	229	8	S235	246	237	3	500	S235	0	**30**	450	S235	50	22	800	4	415
Base Plate Cable Hole Diameter	BPHD0	256	229	8	S235	246	237	3	500	S235	**0**	15	450	S235	50	22	800	4	189
	BPHD60	256	229	8	S235	246	237	3	500	S235	**60**	15	450	S235	50	22	800	4	185
	BPHD150	256	229	8	S235	246	237	3	500	S235	**150**	15	450	S235	50	22	800	4	171
	BPHD200	256	229	8	S235	246	237	3	500	S235	**200**	15	450	S235	50	22	800	4	167
Base Plate Steel Grade	BPSG235	256	229	8	S235	246	237	3	500	**S235**	0	15	450	S235	50	22	800	4	189
	BPSG275	256	229	8	S235	246	237	3	500	**S275**	0	15	450	S235	50	22	800	4	206
	BPSG355	256	229	8	S235	246	237	3	500	**S355**	0	15	450	S235	50	22	800	4	220

Table 3. *Cont.*

Case Study	FE Pole	GFRP Pole Dimensions			Base Sleeve Dimensions					Base Plate Dimensions				Anchor bolts				Peak Impact Force (KN)
	Label	PBD	PTD	PT	BSSG	BSBD	BSTD	BST	BSH	BPSG	BPHD	BPT	BPL	ASG	WD	AD	AL	AN	
		(mm)	(mm)	(mm)		(mm)	(mm)	(mm)	(mm)		(mm)	(mm)	(mm)		(mm)	(mm)	(mm)		
Base Sleeve Height	BSH200	256	229	8	S235	246	241	3	**200**	S235	0	15	450	S235	50	22	800	4	197
	BSH300	256	229	8	S235	246	241	3	**300**	S235	0	15	450	S235	50	22	800	4	216
	BSH400	256	229	8	S235	246	233	3	**400**	S235	0	15	450	S235	50	22	800	4	227
	BSH500	256	229	8	S235	246	237	3	**500**	S235	0	15	450	S235	50	22	800	4	233
Base Sleeve Thickness	BST2	256	229	8	S235	246	237	**2**	500	S235	0	15	450	S235	50	22	800	4	173
	BST3	256	229	8	S235	246	237	**3**	500	S235	0	15	450	S235	50	22	800	4	189
	BST5	256	229	8	S235	246	237	**5**	500	S235	0	15	450	S235	50	22	800	4	199
	BST8	256	229	8	S235	246	237	**8**	500	S235	0	15	450	S235	50	22	800	4	215
Base Sleeve Material	BSSG235	256	229	8	**S235**	246	237	3	500	S235	0	15	450	S235	50	22	800	4	189
	BSSG275	256	229	8	**S275**	246	237	3	500	S235	0	15	450	S235	50	22	800	4	194
	BSSG355	256	229	8	**S355**	246	237	3	500	S235	0	15	450	S235	50	22	800	4	196
Anchor Number	AN4	256	229	8	S235	246	237	3	500	S235	0	30	450	S235	50	22	800	**4**	213
	AN8	256	229	8	S235	246	237	3	500	S235	0	30	450	S235	50	22	800	**8**	312
Anchor Diameter	AD22	256	229	8	S235	246	237	3	500	S235	0	30	450	S235	50	**22**	800	4	173
	AD26	256	229	8	S235	246	237	3	500	S235	0	30	450	S235	50	**26**	800	4	178
	AD30	256	229	8	S235	246	237	3	500	S235	0	30	450	S235	50	**30**	800	4	181
Anchor Material	ASG235	256	229	8	S235	246	237	3	500	S235	0	30	450	**S235**	50	22	800	4	173
	ASG275	256	229	8	S235	246	237	3	500	S235	0	30	450	**S275**	50	22	800	4	178
	ASG355	256	229	8	S235	246	237	3	500	S235	0	30	450	**S355**	50	22	800	4	189
Washer Diameter	WD30	256	229	8	S235	246	237	3	500	S235	0	30	450	S235	**50**	22	800	4	181
	WD40	256	229	8	S235	246	237	3	500	S235	0	30	450	S236	**65**	22	800	4	196
	WD80	256	229	8	S235	246	237	3	500	S235	0	30	450	S237	**80**	22	800	4	206

3.1. GFRP Pole Wall Thickness (PT)

The influence of varying the wall thickness of the GFRP pole was examined by modeling four tapered poles with thicknesses of 6 mm, 8 mm, 10 mm, and 12 mm, as detailed in Table 3. To isolate the effect of wall thickness, the height of the base sleeve was kept constant at 300 mm, allowing the hammer to impact directly on the GFRP wall. All other geometric and material properties were held constant, consistent with the reference configuration. Figure 6a illustrates the impact load–time history curves, highlighting how the pole's wall thickness affects its dynamic response under impact loading. The results confirmed that increasing wall thickness significantly improved energy absorption and dissipation, thereby reducing the force transmitted to vehicle occupants. Figure 6b shows the displacement–time response beneath the hammer, demonstrating that increased wall thickness reduces deformation duration prior to collapse, thereby enhancing energy absorption efficiency. Figure 6c presents the effect of wall thickness on pole toughness, normalized relative to the 6 mm case. Increasing the wall thickness from 6 mm to 12 mm resulted in a decrease in normalized toughness to 24%, indicating a more brittle but controlled failure mode. Additionally, as shown in Figure 6d, thicker poles exhibited faster collapse with reduced deflections, offering a potentially safer impact scenario for passengers.

3.2. GFRP Pole Diameter (PBD)

The effect of varying the GFRP pole's base diameter on its dynamic behavior was investigated by developing models of three tapered poles with base diameters of 184 mm, 256 mm, and 328 mm, as listed in Table 3. All other geometric and material properties were kept consistent with the reference configuration. Figure 7a presents the impact load–time history curves, demonstrating the influence of base diameter on the dynamic response of the GFRP pole. Figure 7b shows the corresponding displacement–time histories at the point directly beneath the hammer. To evaluate pole toughness, normalized values were calculated relative to the 184 mm base diameter case, as shown in Figure 7c. Increasing the base diameter from 184 mm to 256 mm resulted in a stiffer response, reducing the normalized toughness to 63%. Furthermore, as illustrated in Figure 7d, the 256 mm pole underwent a more rapid collapse with lower deflection, facilitating quicker energy dissipation during impact.

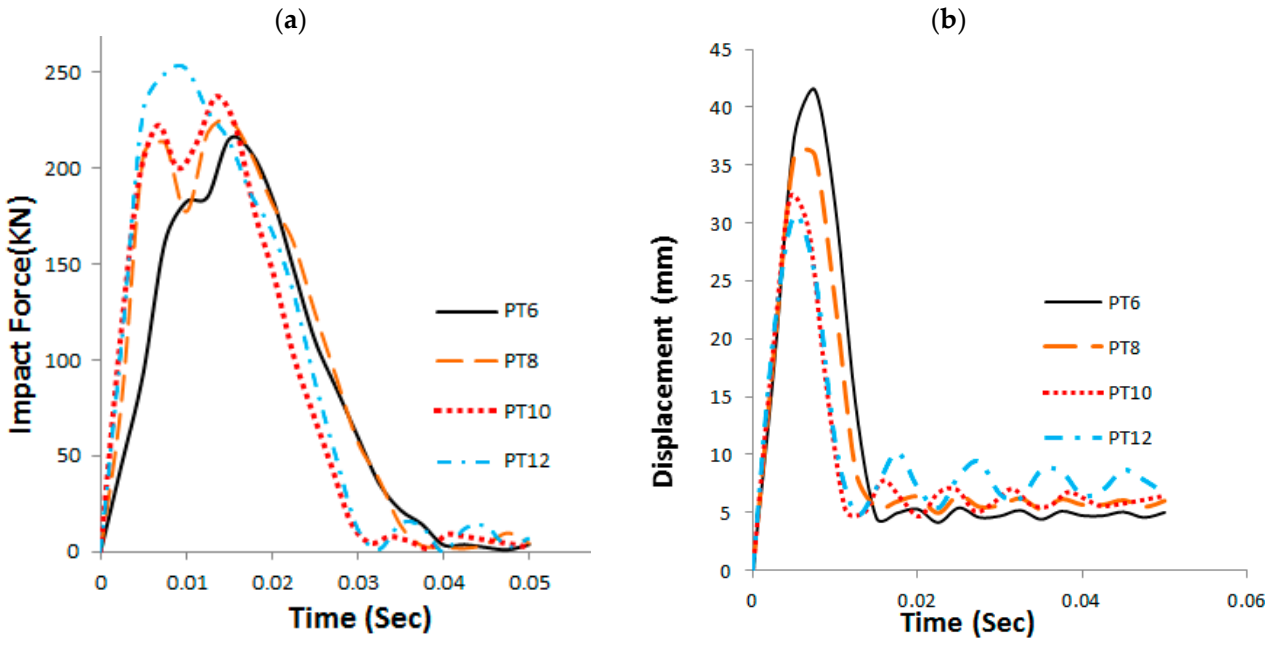

Figure 6. *Cont.*

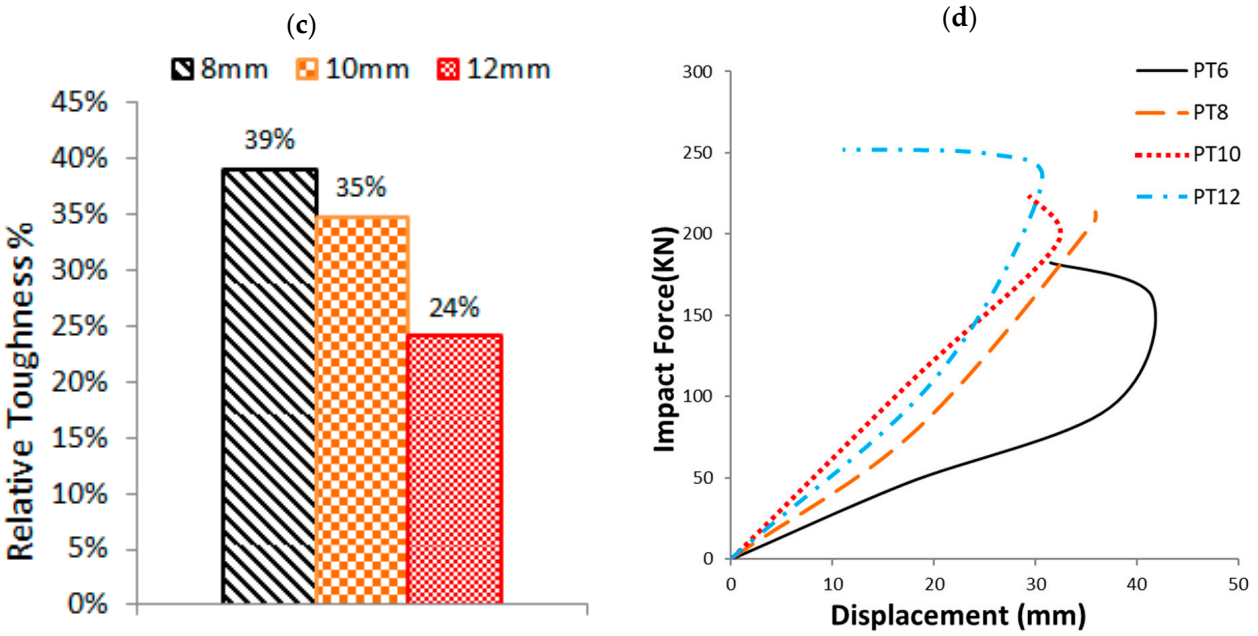

Figure 6. The effect of the GFRP pole wall thickness: (**a**) the impact force time history, (**b**) the pole deflection time history, (**c**) the normalized toughness of the studied cases of different GFRP wall thicknesses, and (**d**) impact force—displacement curves of the GFRP poles having different wall thicknesses.

3.3. Base Plate Dimensions (L and B)

The dimensions of the base plate, specifically its length (L) and width (B), were varied with values of 450 mm, 500 mm, 550 mm, and 600 mm, as listed in Table 3. Figure 8 illustrates the von Mises stress distribution across the deformed base plates for the 450 mm and 600 mm configurations. Increasing the base plate dimensions caused plastic deformation to occur in the steel sleeve before the base plate yielded.

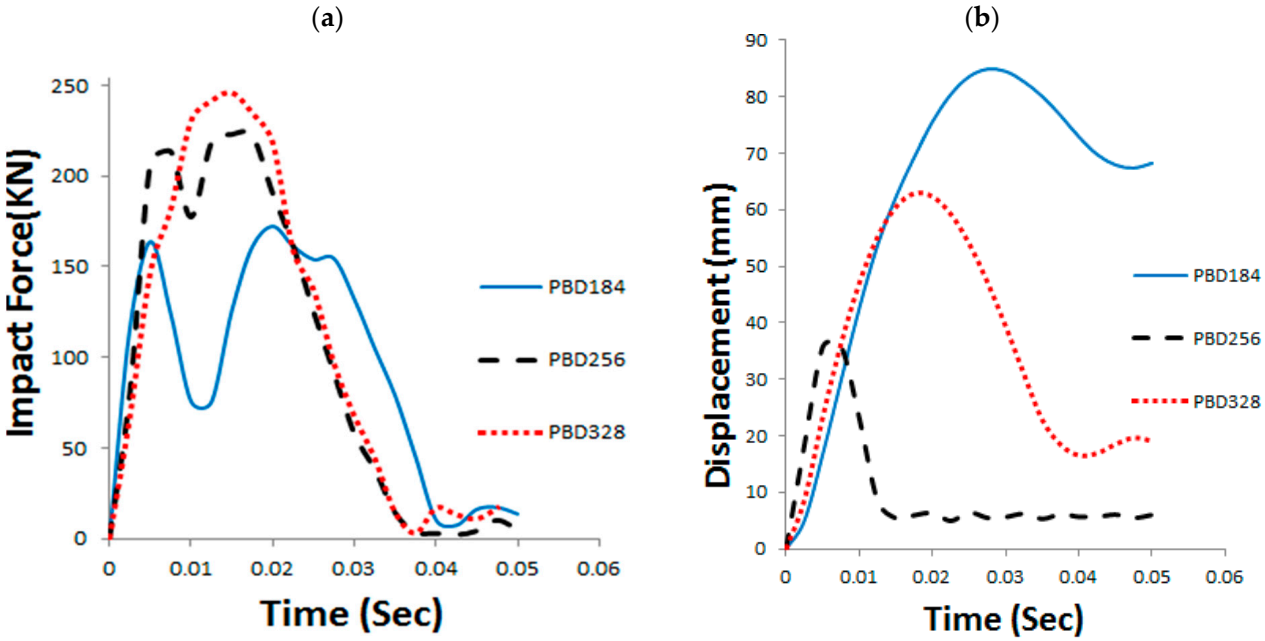

Figure 7. *Cont.*

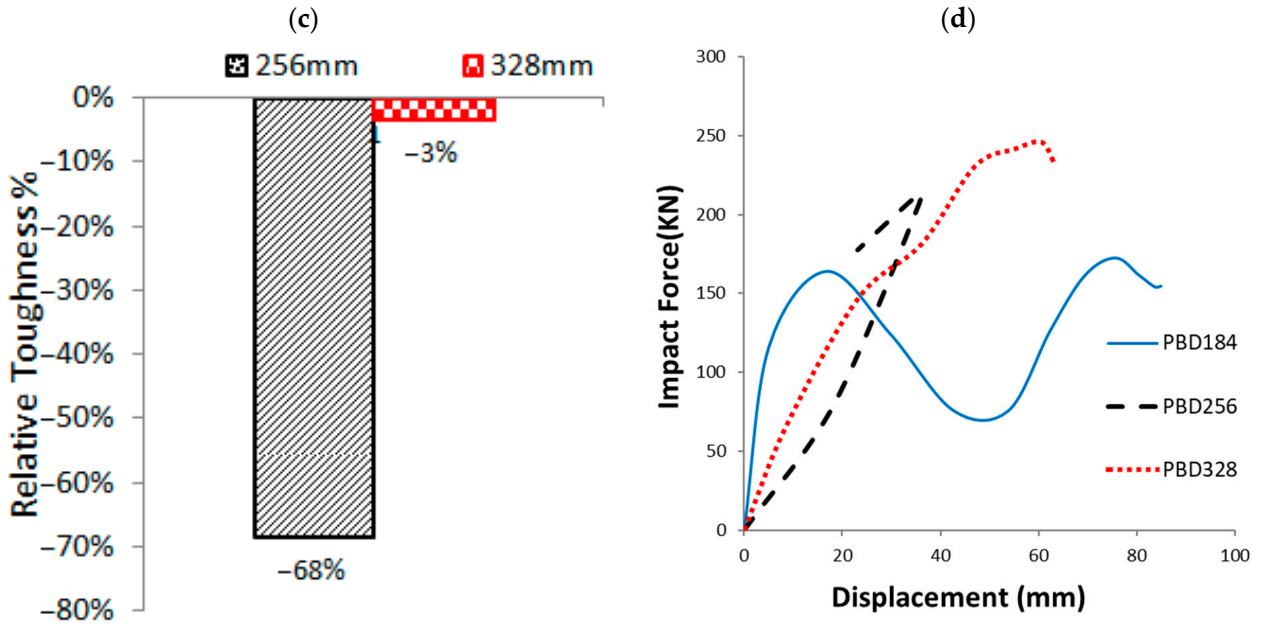

Figure 7. The effect of the GFRP pole bottom diameter: (**a**) the impact force time history, (**b**) the pole deflection time history, (**c**) the normalized toughness of the GFRP poles with different bottom diameters, and (**d**) impact force—displacement curves of the GFRP poles having different bottom wall diameters.

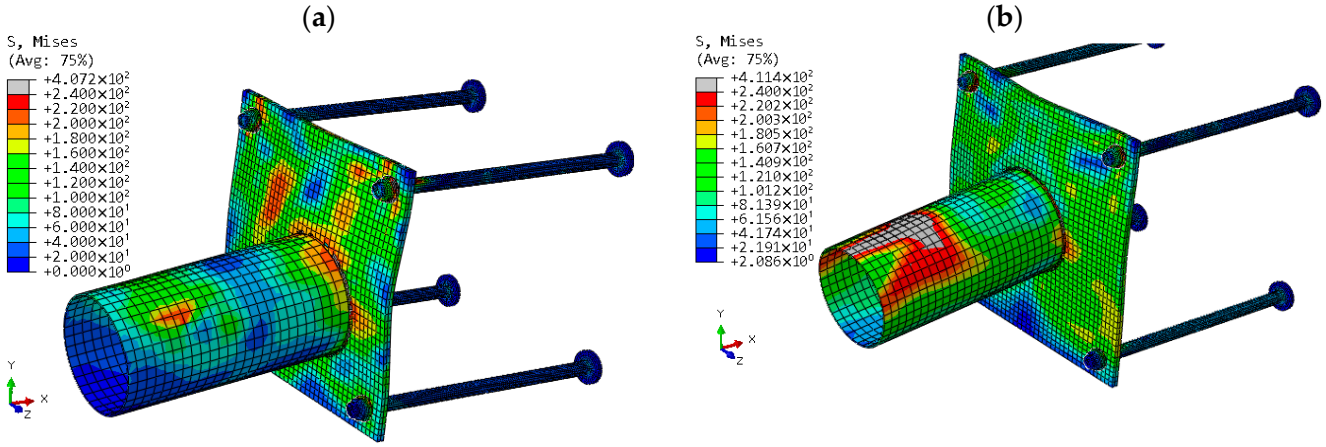

Figure 8. The von Mises stress distribution of the base plate and base sleeve: (**a**) BPL450 and (**b**) BPL600.

This resulted in a more favorable energy dissipation scenario, compared to cases where the base plate yielded first and experienced plastic deformation between the two tension-side anchor bolts, as reflected in the impact force curves in Figure 9a. The influence of base plate dimensions on pole deflection is presented in Figure 9b, showing the displacement–time history at the point beneath the hammer. Normalized pole toughness was calculated relative to the 450 mm base plate case, as shown in Figure 9c. Enlarging the base plate from 450 mm to 600 mm resulted in a stiffer structural response and shifted the plastic deformation to the sleeve, reducing the normalized toughness to 35%. As shown in Figure 9d, increasing base plate dimensions led to faster collapse with lower deflections, thereby contributing to a safer impact outcome for passengers.

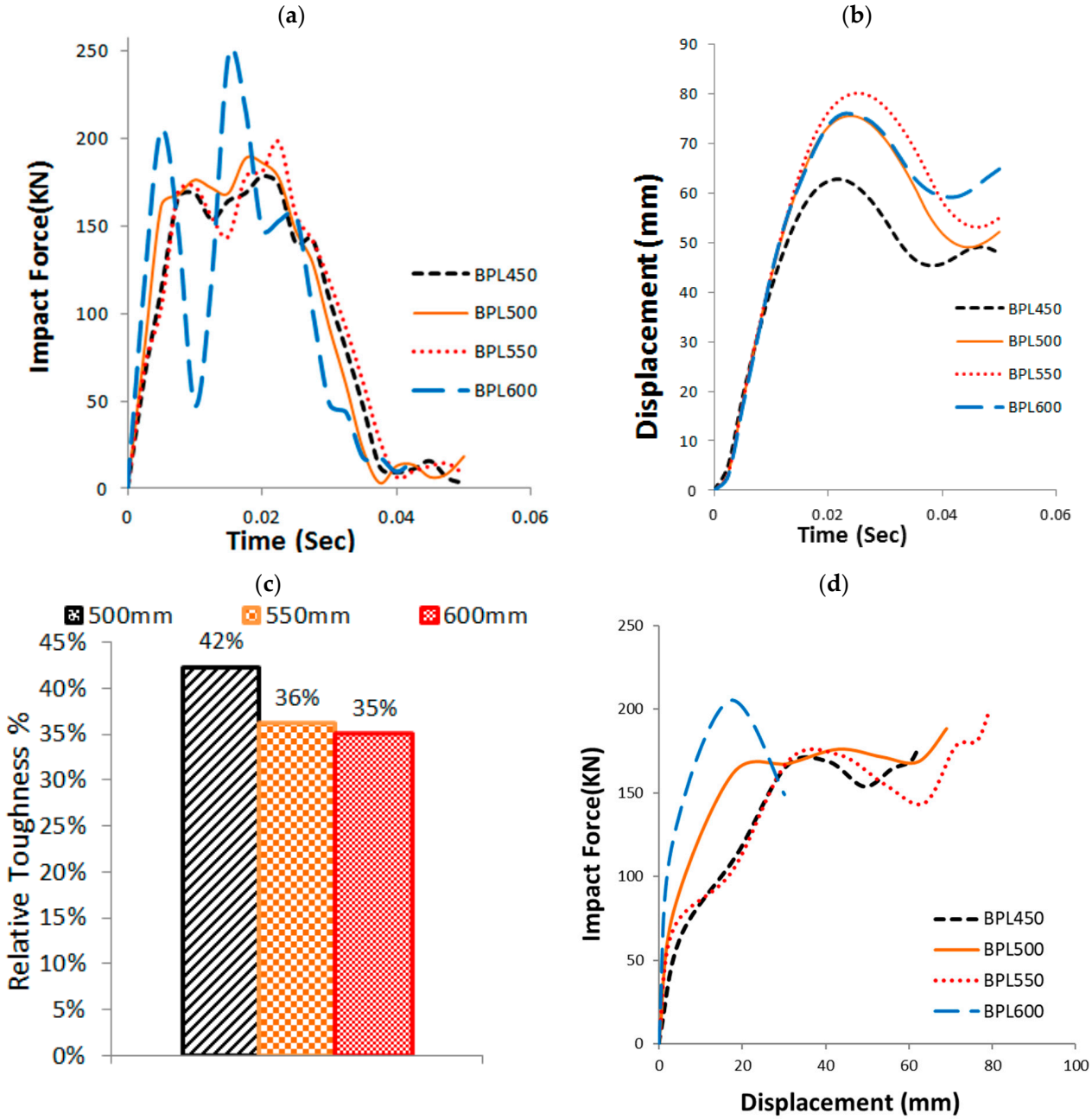

Figure 9. The effect of the GFRP poles with different base plate: (**a**) the impact force time history, (**b**) the pole deflection time history, (**c**) the normalized toughness of the studied cases with different base plate dimensions, and (**d**) impact force—displacement curves of the GFRP poles having different base plate plane dimensions (mm).

3.4. Base Plate Thickness (T)

Four tapered GFRP pole specimens were simulated to investigate the effect of varying base plate thicknesses: 10 mm, 15 mm, 20 mm, and 30 mm, as listed in Table 3. Figure 10 presents the von Mises stress distribution in the deformed base plates for selected thicknesses (10 mm, 20 mm, and 30 mm).

The effect of base plate thickness on the peak impact force over time is illustrated in Figure 11a, while Figure 11b displays the corresponding displacement–time history beneath the hammer.

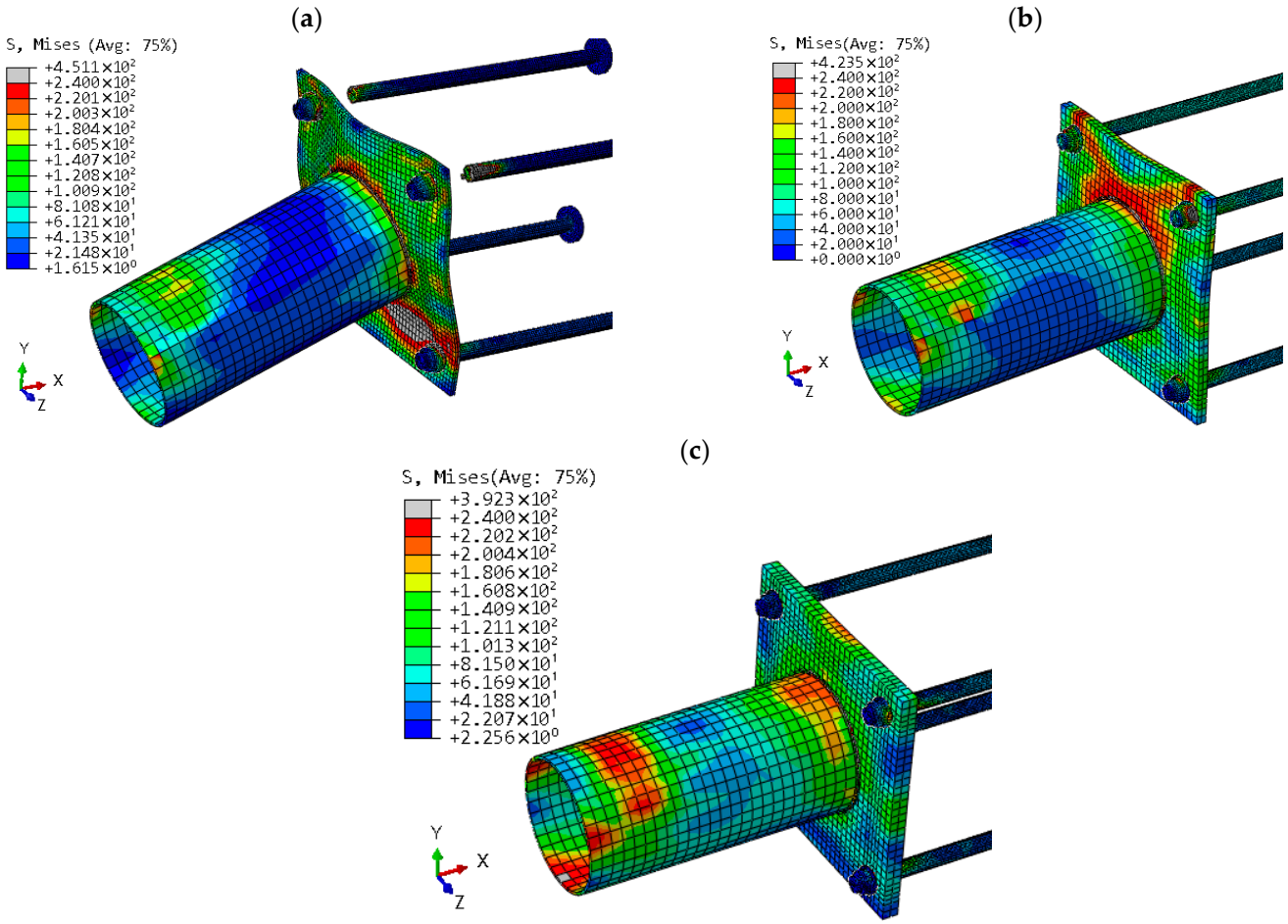

Figure 10. The von Mises stress distribution of the base plate and base sleeve: (**a**) BPT10, (**b**) BPT20, and (**c**) BPT30.

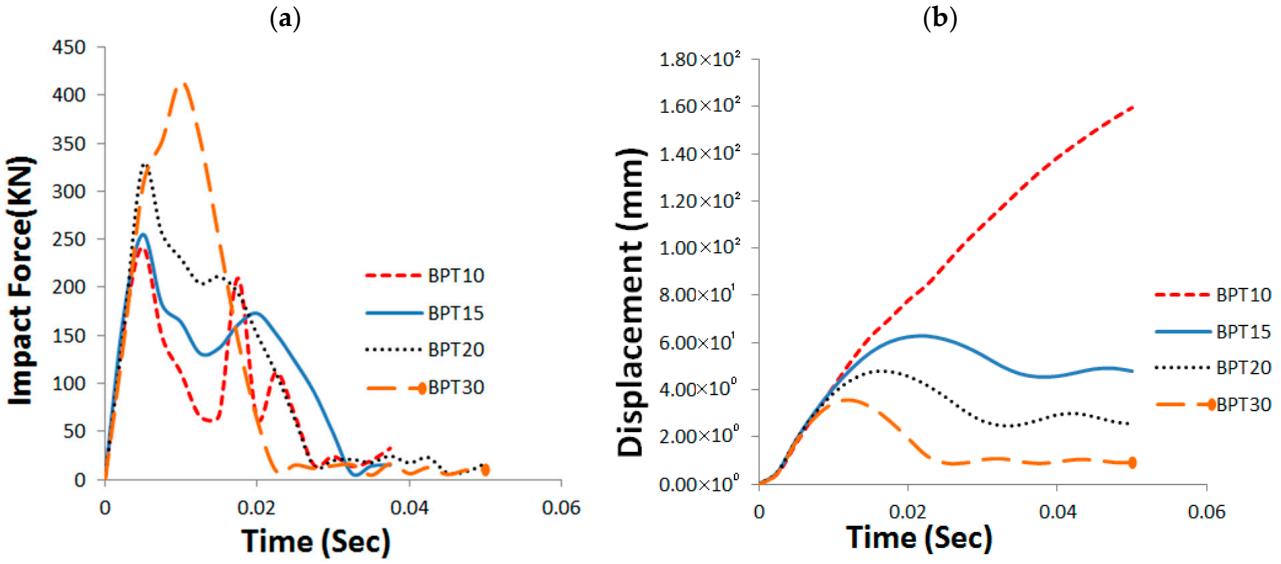

Figure 11. *Cont.*

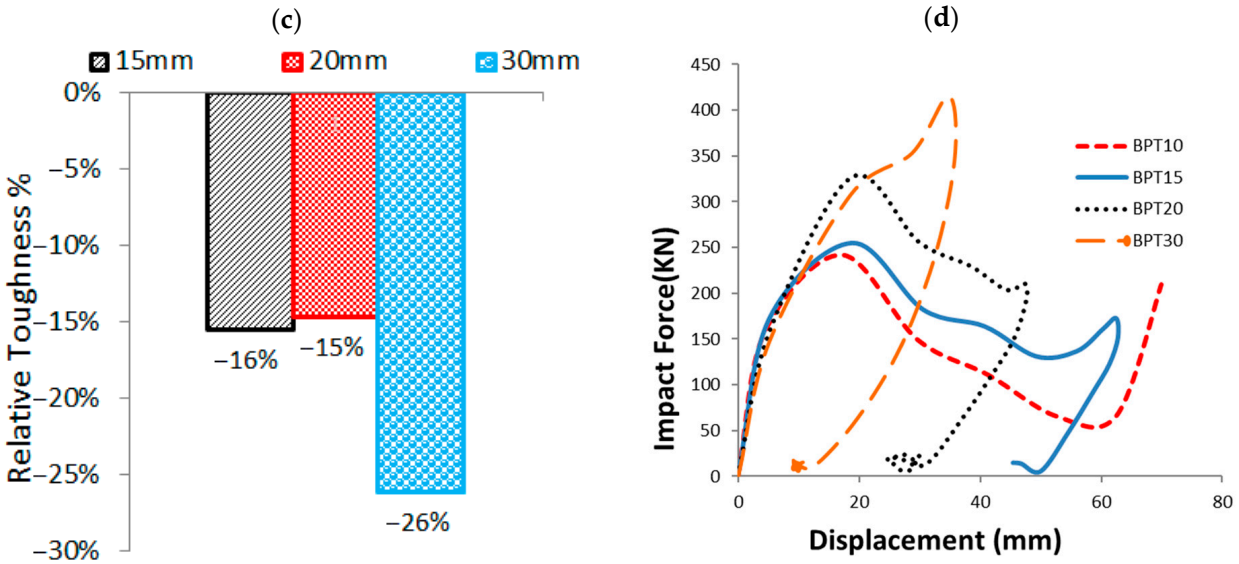

Figure 11. The effect of the GFRP poles with different base plate thickness: (**a**) the impact force time history, (**b**) the pole deflection time history, (**c**) normalized pole toughness of the studied cases with different base plate thicknesses, and (**d**) impact force—displacement curves of the GFRP poles having different base plate plane thicknesses (mm).

Varying the base plate thickness produced distinct effects on deformation capacity and energy absorption prior to failure. Thinner base plates experienced greater deformations, enhancing overall toughness while reducing the initial peak impact force. This trend is evident in Figure 11c, which presents normalized pole toughness relative to the 10 mm base plate case. A notable reduction in normalized toughness—approximately 26%—was observed as the thickness increased from 10 mm to 30 mm. In thinner base plates, plastic deformation was concentrated on the compression side, while tensile failure occurred in the anchor bolts on the tension side. As shown in Figure 11d, poles with thicker base plates failed more quickly and with minimal deflection, contributing to a safer impact scenario for passengers.

3.5. Electric Cable Hole Diameter (HD)

The effect of varying the electric cable hole diameter in the base plate was investigated using three values: 60 mm, 150 mm, and 200 mm. The von Mises stress distribution for the analyzed cases is presented in Figure 12, showing increased stress concentrations around the hole as the diameter increased.

Larger hole diameters of 150 mm and 200 mm led to more pronounced deformation and reduced stiffness compared to the 60 mm hole, as illustrated in Figure 13a. This increased deformation around the hole region also contributed to weld failure in the base plate for the larger diameters.

Figure 13b presents the displacement–time histories of the GFRP poles for each hole diameter configuration. In terms of normalized pole toughness, Figure 13c shows that enlarging the hole diameter to 150 mm and 200 mm resulted in increases of 36.44% and 36.46%, respectively, compared to poles without an electric cable hole. In contrast, the 60 mm hole yielded only a 10.65% increase. As highlighted in Figure 13d, the cable hole diameter had a relatively minor effect on the overall toughness of the GFRP poles.

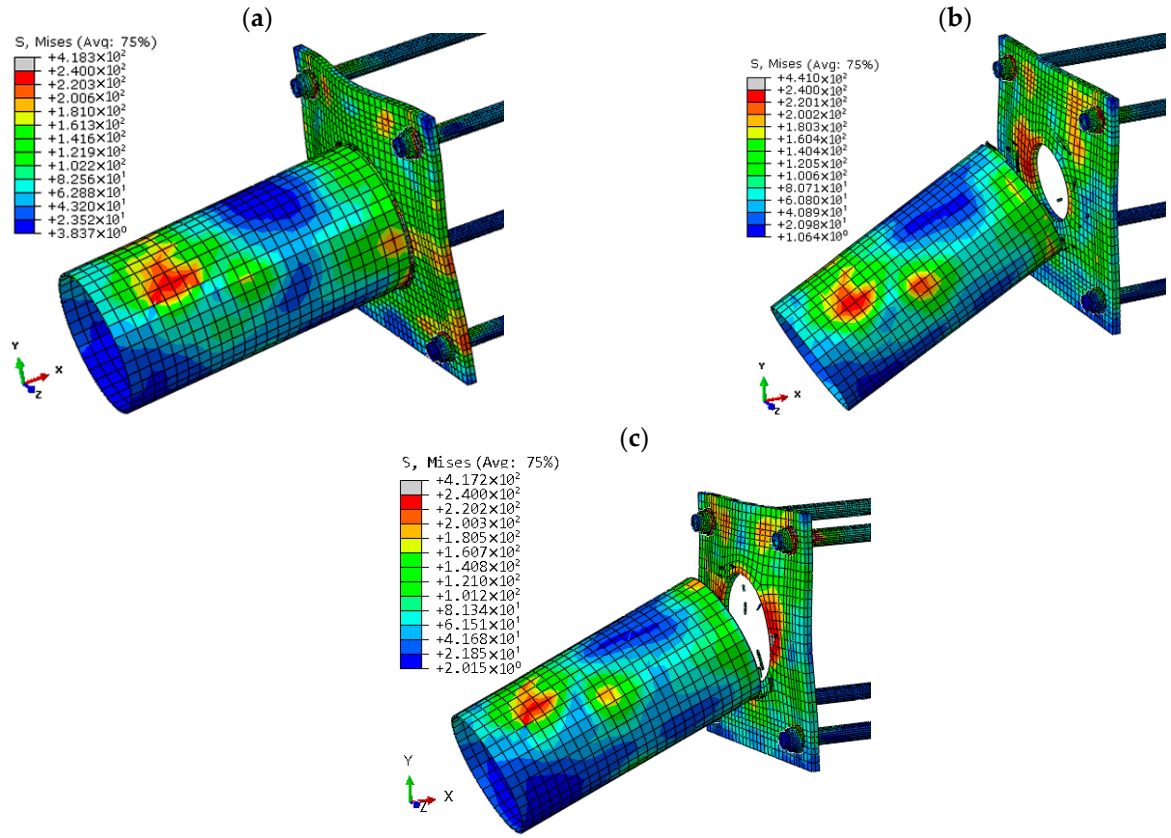

Figure 12. The von Mises stress distribution of the base plate with cable hole: (**a**) BPHD60, (**b**) BPHD150, and (**c**) BPHD200.

3.6. Base Plate Material Properties (SG)

The structural response was examined by varying the steel grade of the base plate, specifically using S235, S275, and S355 grades, as listed in Table 3. Transitioning from mild to high-strength steel resulted in a stiffer response and higher initial peak impact forces under impact loading. In contrast, the use of mild steel led to lower peak forces and greater ductility, as shown in Figure 14a. The influence of base plate material on pole deflection is presented in Figure 14b, displaying the displacement–time history at the point beneath the hammer.

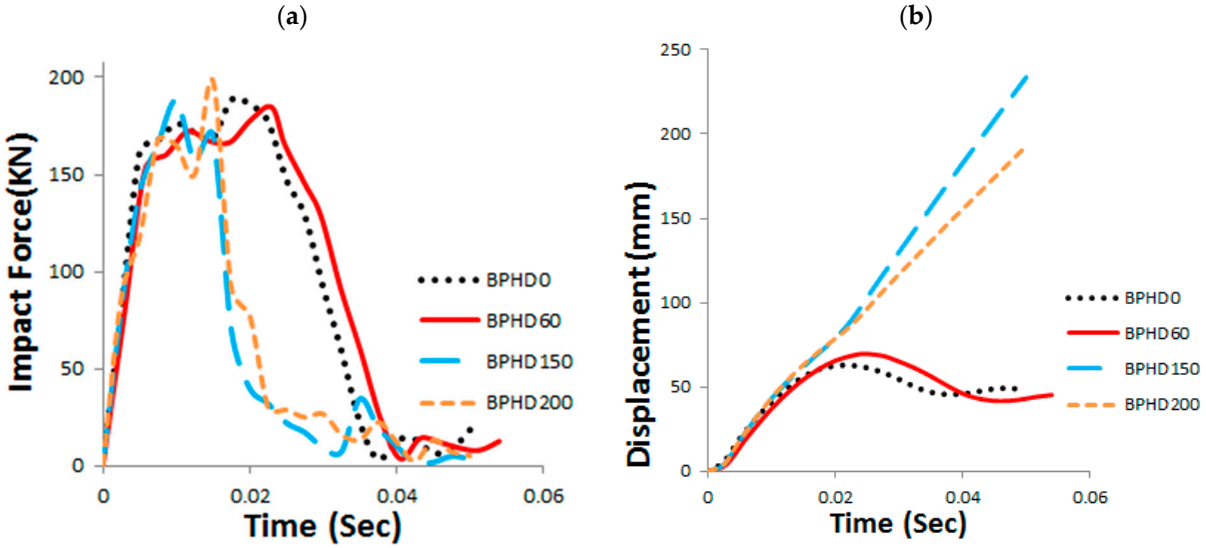

Figure 13. *Cont.*

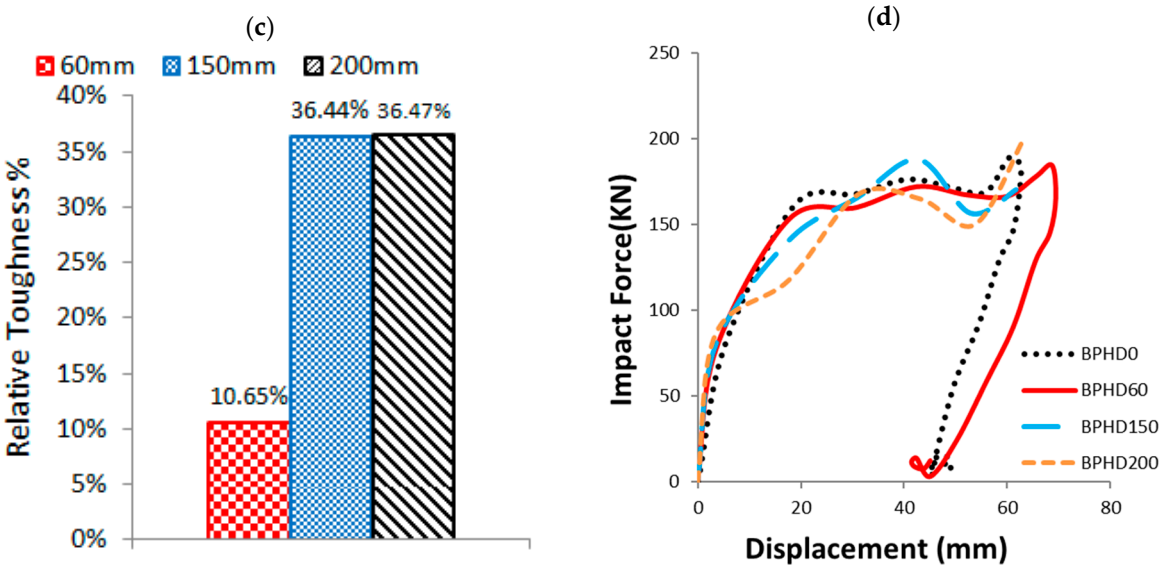

Figure 13. The effect of the GFRP poles with different base plate cable hole diameter: (**a**) the impact force time history, (**b**) the pole deflection time history, (**c**) normalized pole toughness of the studied cases with different base plate cable hole diameter, and (**d**) impact force—displacement curves of the GFRP poles having different cable hole diameters (mm).

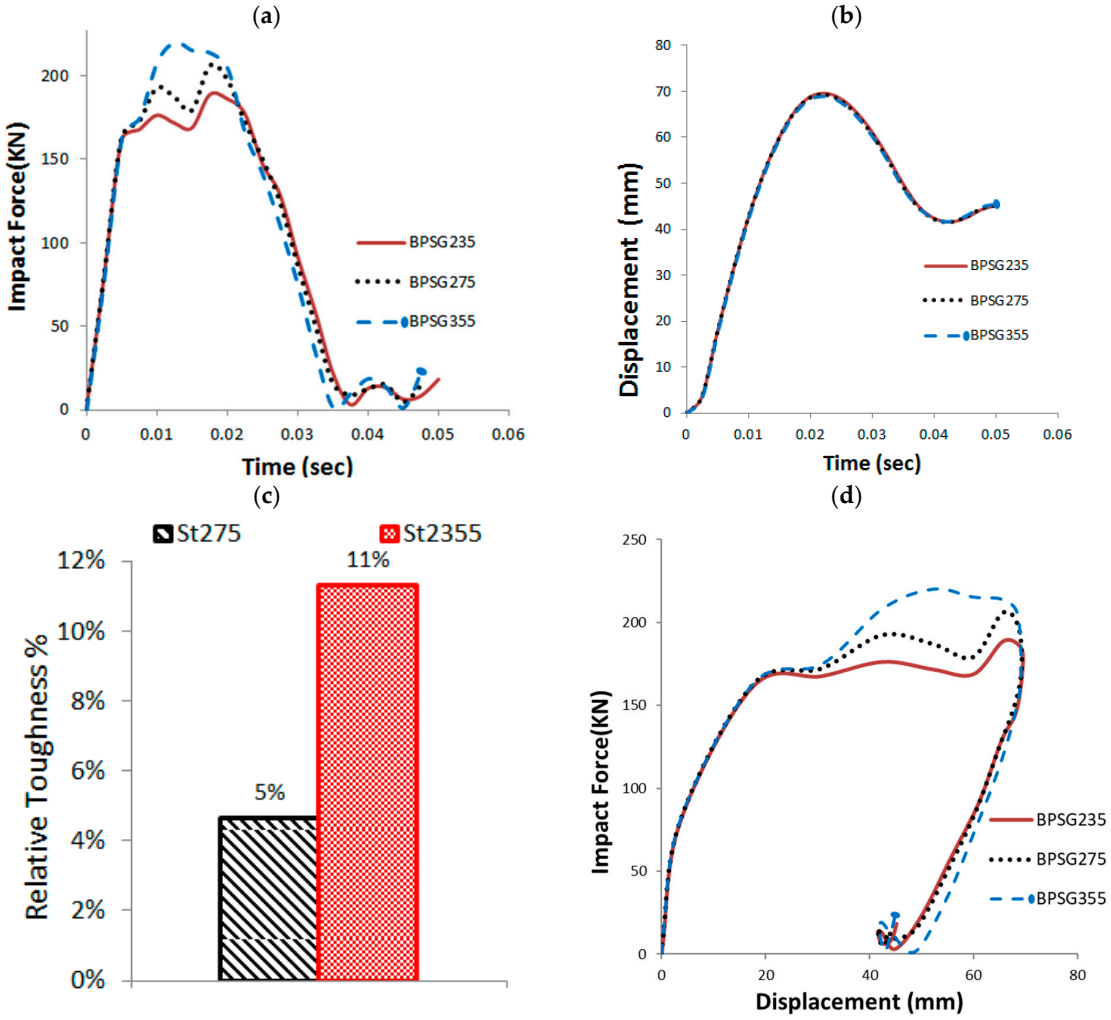

Figure 14. The effect of the GFRP poles with different base plate material: (**a**) the impact force time history, (**b**) the pole deflection time history, (**c**) normalized pole toughness of the studied cases with

different base plate material, and (**d**) impact force—displacement curves of the GFRP poles having different material grade (MPa).

Figure 14c illustrates the variation in normalized toughness of the GFRP poles with different base plate materials, using the S235 grade as a reference. The use of S355 steel resulted in an 11% increase in normalized toughness. As shown in Figure 14d, poles with the lowest-grade steel exhibited quicker collapse and more effective energy dissipation, contributing to a potentially safer impact scenario.

3.7. Base Sleeve Height (BSH)

Four tapered GFRP poles with varying base sleeve heights were examined, as detailed in Table 3. Changing the height of the base sleeve had a clear impact on the initial peak impact force, as shown in Figure 15a. When the sleeve height was reduced to 200 mm, the hammer impacted the GFRP pole above the steel sleeve. This configuration resulted in the lowest initial peak impact force and extended the deformation period before reaching that peak, which helped disperse impact energy and mitigate the severity of the collision on the impacting vehicle.

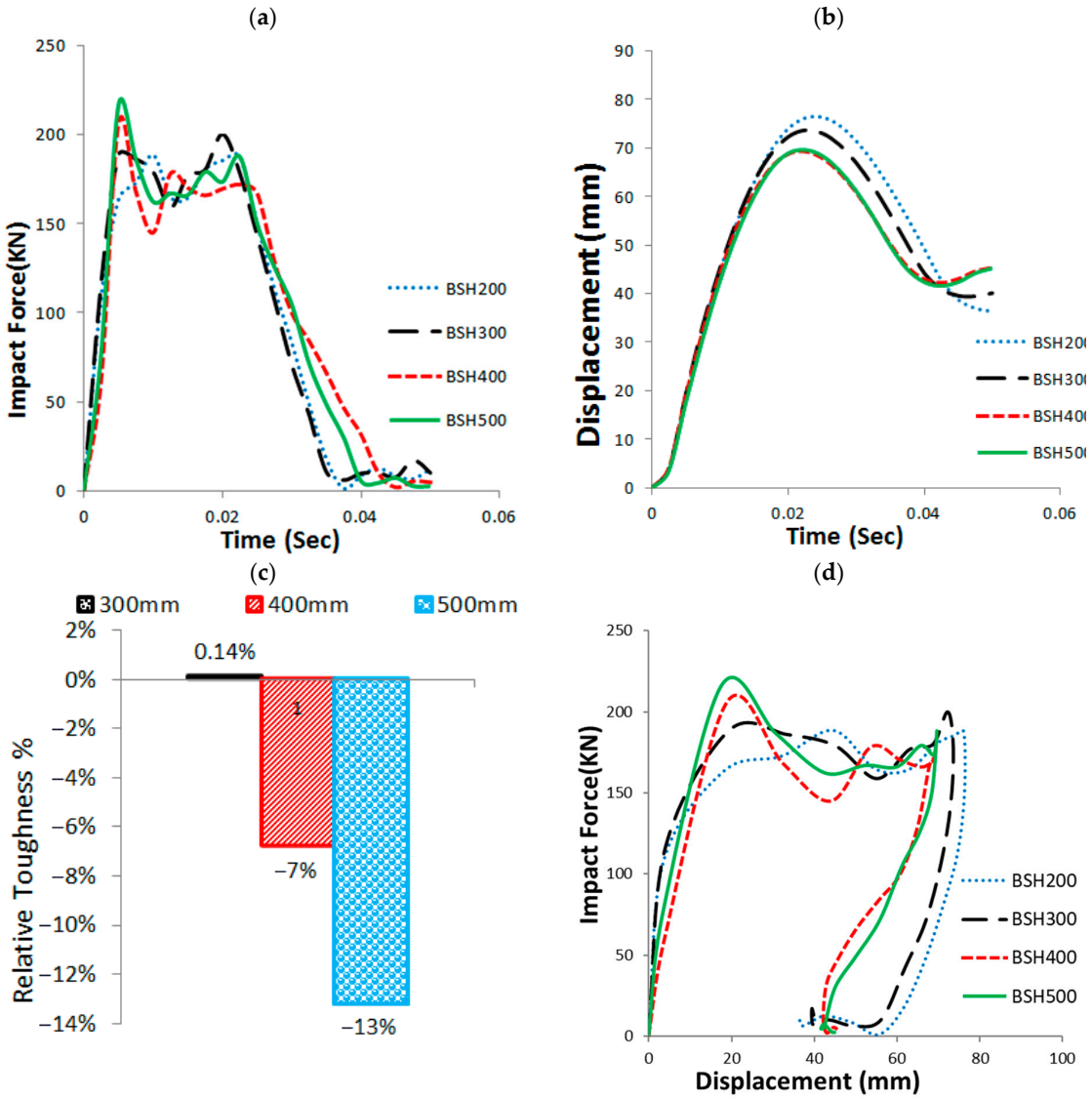

Figure 15. The effect of the GFRP poles with different base sleeve height: (**a**) the impact force time history, (**b**) the pole deflection time history, (**c**) normalized pole toughness of the studied cases with different base sleeve height, and (**d**) impact force—displacement curves of the GFRP poles having different sleeve height (mm).

The effect of base sleeve height on pole deflection is shown in Figure 15b, through the displacement–time history at the point beneath the hammer. Figure 15c presents the normalized pole toughness relative to the 200 mm sleeve height case. Increasing the sleeve height led to a reduction in normalized toughness, with decreases of up to 13% observed at a height of 500 mm. Additionally, Figure 15d highlights that taller base sleeves contributed to quicker failure of the poles, indicating reduced energy absorption capacity.

3.8. Base Sleeve Thickness (BST)

In this study, the effect of varying the base sleeve thickness was investigated using values of 2 mm, 3 mm, 5 mm, and 8 mm, as detailed in Table 3. The base sleeve thickness had a significant influence on the initial peak impact force, as illustrated in Figure 16a. The thinnest sleeve (2 mm) exhibited the lowest peak impact force and showed a delayed response in reaching this force, indicating a more gradual energy absorption process.

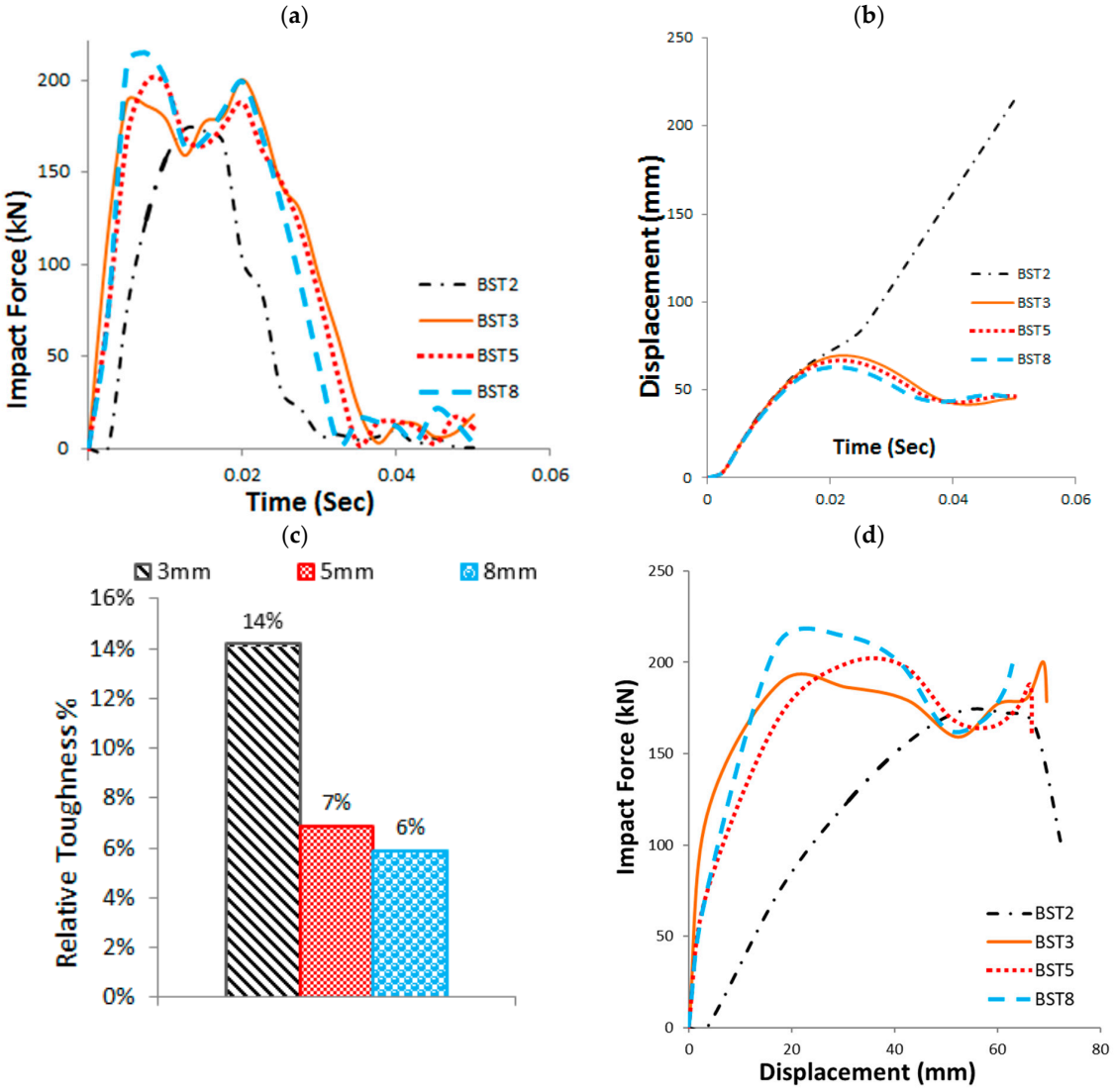

Figure 16. The effect of the GFRP poles with different base sleeve thicknesses: (**a**) the impact force time history, (**b**) the pole deflection time history, (**c**) normalized pole toughness of the studied cases with different base sleeve thicknesses, and (**d**) impact force—displacement curves of the GFRP poles having different base sleeve thicknesses (mm).

The influence of sleeve thickness on pole deflection is shown in Figure 16b, presenting the displacement–time history at the point beneath the hammer. Figure 16c displays

the normalized pole toughness relative to the 2 mm sleeve thickness. Increasing the sleeve thickness from 3 mm to 8 mm led to a 7% reduction in normalized toughness. As highlighted in Figure 16d, base sleeve thicknesses greater than 3 mm had minimal additional effect on the dynamic response, suggesting a threshold beyond which further thickening offers limited benefits.

3.9. Base Sleeve Material Properties (SG)

This study examined the effect of varying the steel grade of the base sleeve using European structural steel grades S235, S275, and S355, as detailed in Table 3. Changing the base sleeve material from mild to high-strength steel had a marginal effect on the overall structural behavior and the initial peak impact force, as shown in Figure 17a. The influence of base sleeve material properties on pole deflection is presented in Figure 17b, which shows the displacement time–time history at the point beneath the hammer. Figure 17c displays the normalized toughness of the GFRP poles with different base sleeve materials, relative to the S235 grade. A slight increase of 1.14% in normalized toughness was observed when S355 steel was used. As highlighted in Figure 17d, the grade of the steel sleeve had minimal impact on the finite element analysis results.

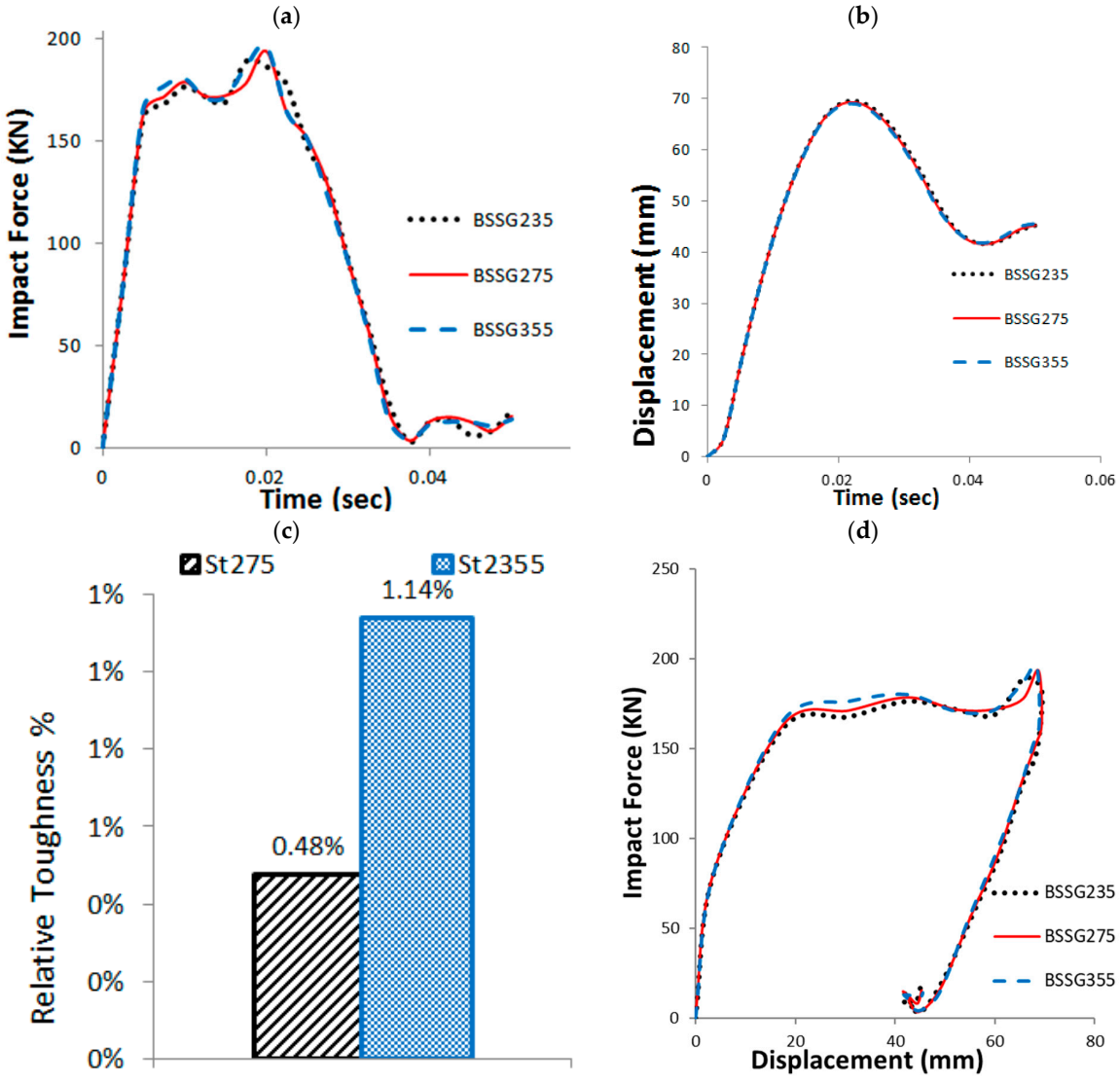

Figure 17. The effect of the GFRP poles with different base sleeve material properties (steel grade): (**a**) the impact force time history, (**b**) the pole deflection time history, (**c**) normalized pole toughness

of the studied cases with different base sleeve material properties (steel grade), and (**d**) impact force—displacement curves of the GFRP poles having different grades for the steel sleeve (MPa).

3.10. Anchor Bolts Patterns (AN)

The impact of anchor bolt quantity was investigated by analyzing two configurations: four bolts and eight bolts, as detailed in Table 3. The anchor arrangements for both cases are illustrated in Figure 18. Employing eight anchor bolts (three on each side of the base plate) had a significant effect on the initial peak impact force, as shown in Figure 19a. The influence of anchor bolt configuration on pole deflection is presented in Figure 19b through the displacement–time history beneath the hammer.

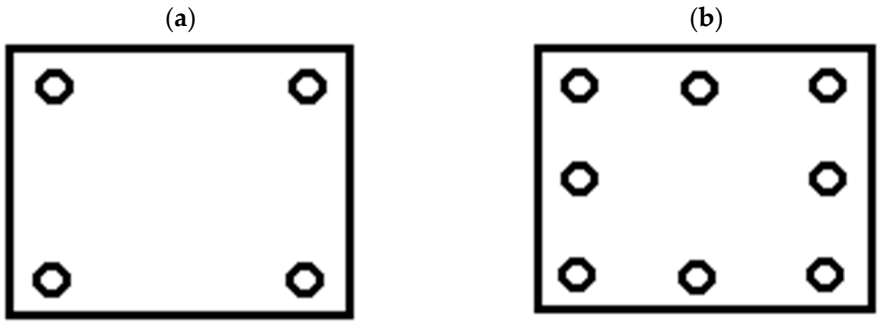

Figure 18. Anchor bolts arrangement for two cases: (**a**) four bolts and (**b**) eight bolts.

Using eight anchor bolts enhanced the fixation of the pole, restricted base plate deformation, and prevented rotational movement. As a result, a stiffer structural response was observed, and the pole's normalized toughness increased by 11%, as depicted in Figure 19c. In the eight-bolt configuration, the impact was concentrated on the steel sleeve beneath the hammer, leading to a weld fracture between the sleeve and the base plate. Minimal base plate deformation was observed due to the restraint provided by the three bolts on each side. Consequently, the sleeve and weld governed the dynamic response, resulting in quicker failure of the GFRP pole compared to the four-bolt pattern.

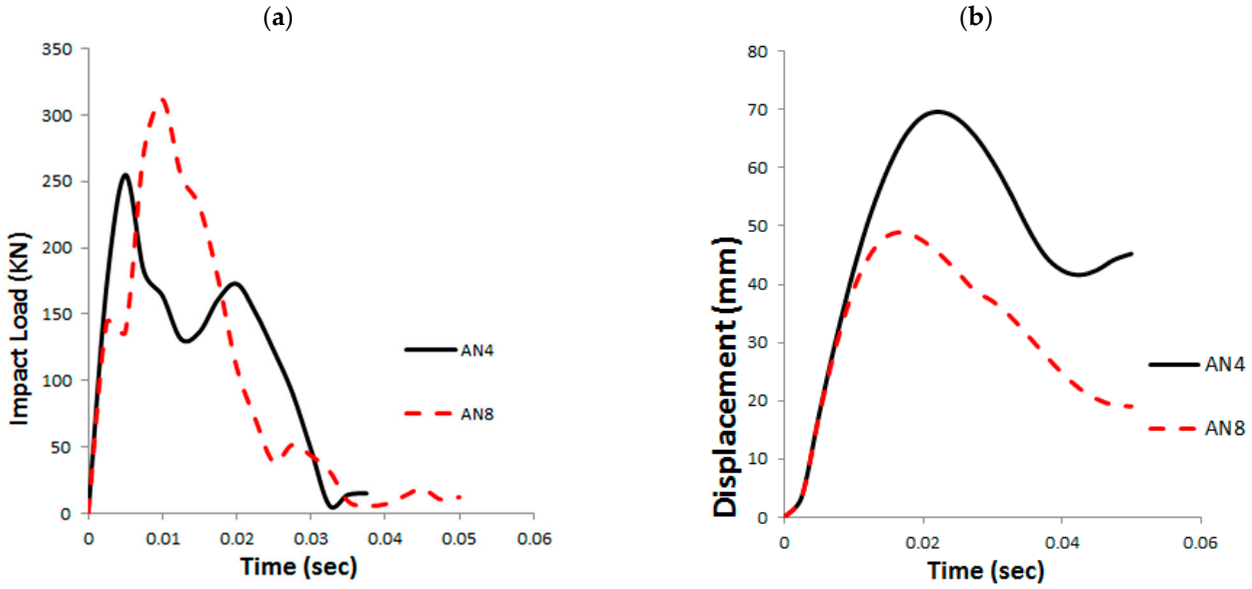

Figure 19. *Cont.*

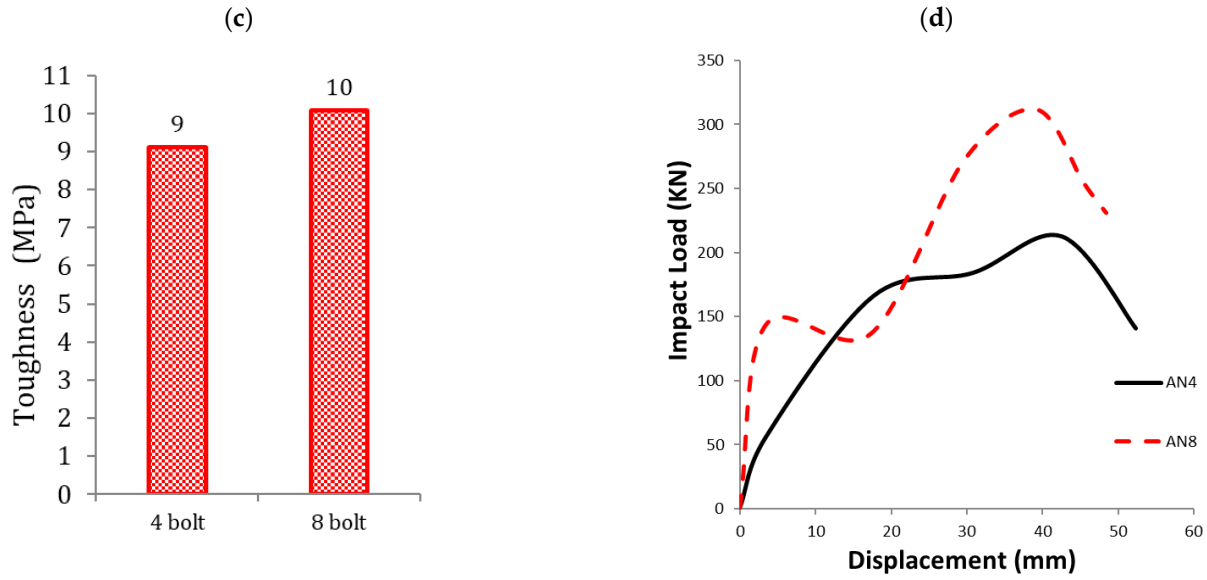

Figure 19. The effect of the GFRP poles with different anchor bolts patterns (AN): (**a**) the impact force time history, (**b**) the pole deflection time history, (**c**) normalized pole toughness of the studied cases with different anchor bolts patterns (AN), and (**d**) impact force—displacement curves of the GFRP poles having different anchor bolts patterns (AN).

Figure 19d demonstrates that although both configurations show similar global responses, the four-bolt arrangement allows for more energy dissipation and delayed failure. This behavior may provide improved safety for passengers by mitigating the severity of impact through greater deformation capacity. The von Mises stress distribution for the deformed configurations is shown in Figure 20.

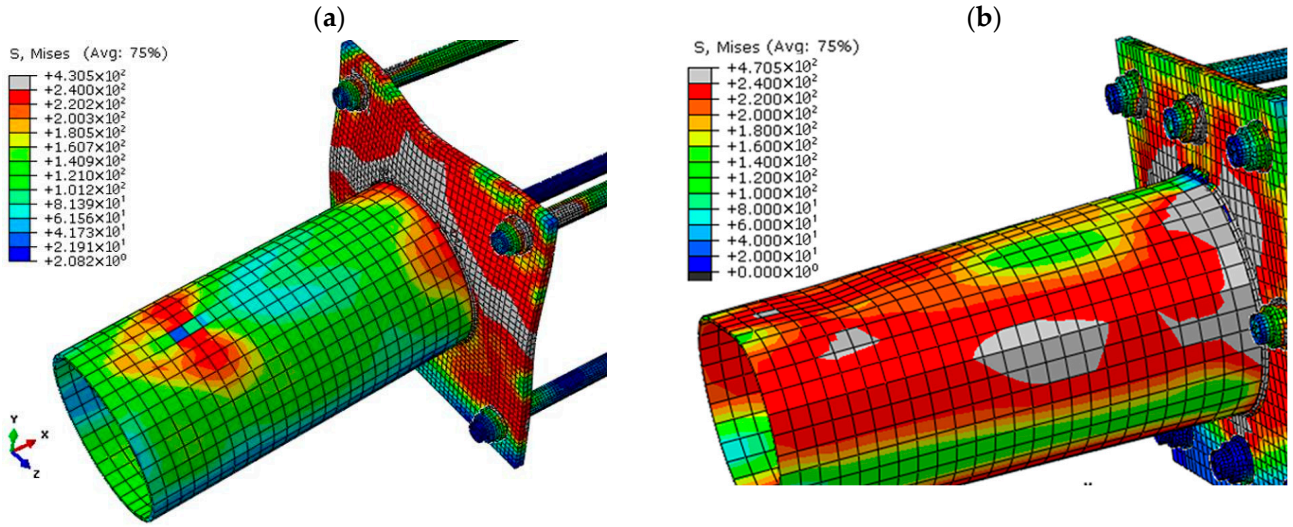

Figure 20. The von Mises stress distribution of the base plate and base sleeve: (**a**) four bolts and (**b**) eight bolts.

3.11. Anchor Bolts Diameter (AD)

The effect of anchor bolt diameter on the structural response of GFRP poles was investigated using three values: 22 mm, 26 mm, and 30 mm. Increasing the anchor bolt diameter had a minimal influence on overall pole deformation, as shown in Figure 21a. The displacement–time history at the point beneath the hammer, presented in Figure 21b, illustrates the impact of bolt diameter on pole deflection.

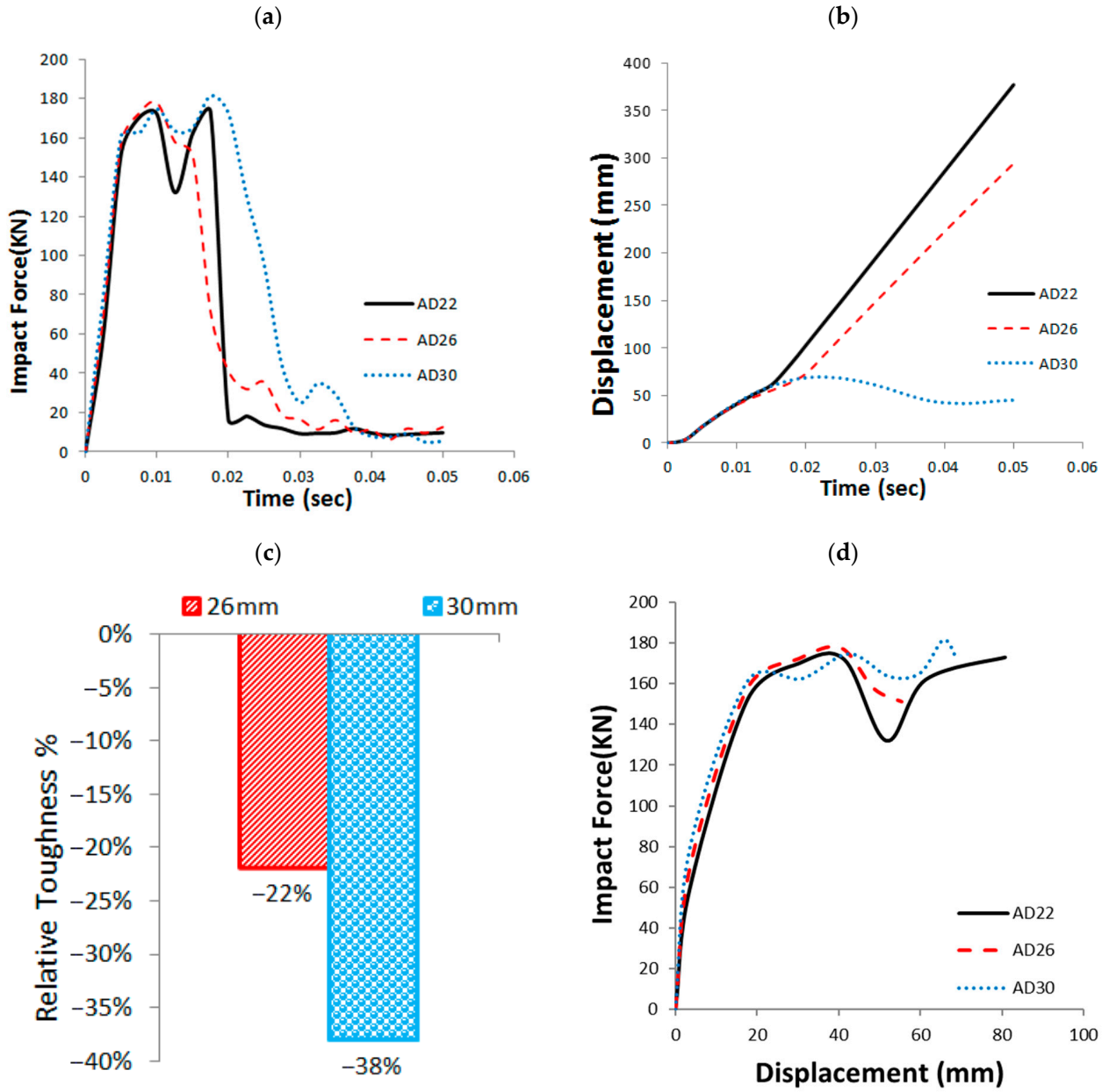

Figure 21. The effect of the GFRP poles with different anchor bolt diameter (AD): (**a**) the impact force time history, (**b**) the pole deflection time history, (**c**) normalized pole toughness of the studied cases with different anchor bolt diameter (AD), and (**d**) impact force—displacement curves of the GFRP poles having different anchor bolts diameters (mm).

Figure 21c shows the normalized toughness of GFRP poles with different anchor bolt diameters, using the 22 mm case as the reference. A significant reduction in normalized toughness was observed with increasing bolt diameter: 22% for 26 mm bolts and 32% for 30 mm bolts. As highlighted in Figure 21d, larger anchor bolt diameters reduce the energy absorption capacity of the poles, leading to lower toughness under impact loading conditions.

3.12. Anchor Bolts Material Properties (ASG)

This section evaluates the influence of anchor bolt material strength—specifically steel grades S235, S275, and S355 (as outlined in Table 3)—on the dynamic response of GFRP poles. Transitioning from mild to high-strength steel showed minimal impact on the initial peak impact force but led to a significant increase in both the ultimate peak impact force

and impact force duration (see Figure 22a). The displacement time history at the point beneath the hammer, shown in Figure 22b, highlights the effect of material grade on pole deflection. Figure 22c presents the normalized toughness of poles with different anchor bolt grades, benchmarked against S235. A toughness reduction of 8% was observed when using S355. Figure 22d further demonstrates the limited variation in FE results attributable to changes in anchor bolt material grade.

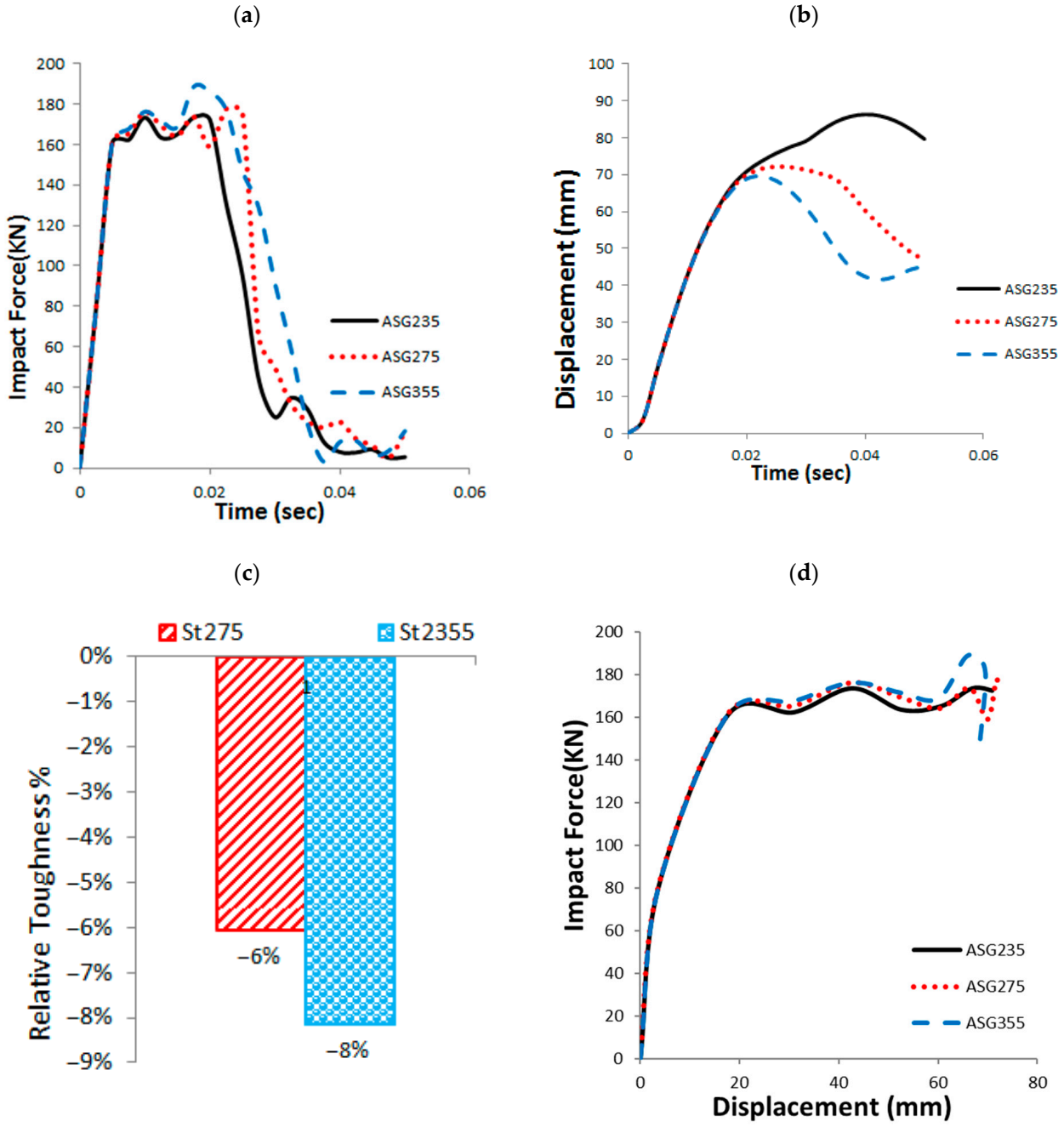

Figure 22. The effect of the GFRP poles with different anchor bolts materials (steel grade): (**a**) the impact force time history, (**b**) the pole deflection time history, (**c**) normalized pole toughness of the studied cases with different anchor bolts materials, and (**d**) impact force—displacement curves of the GFRP poles having different anchor bolts grades (MPa).

3.13. Washer Diameter (WD)

The effect of steel anchor washer diameter was investigated using 50 mm, 65 mm, and 80 mm washers (Table 3). As shown in Figure 23a, increasing the washer diameter

led to a notable rise in both the peak impact force and the duration of the impact. The displacement–time history beneath the hammer (Figure 23b) revealed that larger washers reduced pole deflection. Figure 23c presents the normalized toughness of GFRP poles relative to the 50 mm washer case, indicating a 12% reduction in toughness with an 80 mm washer. Figure 24 illustrates the von Mises stress distribution, confirming that larger washers enhance base plate fixation, structural stiffness, and impact resistance. However, this comes at the cost of lower energy absorption and reduced pole toughness. Figure 23d highlights the significance of washer diameter on GFRP pole response, with direct implications for passenger safety under impact loading.

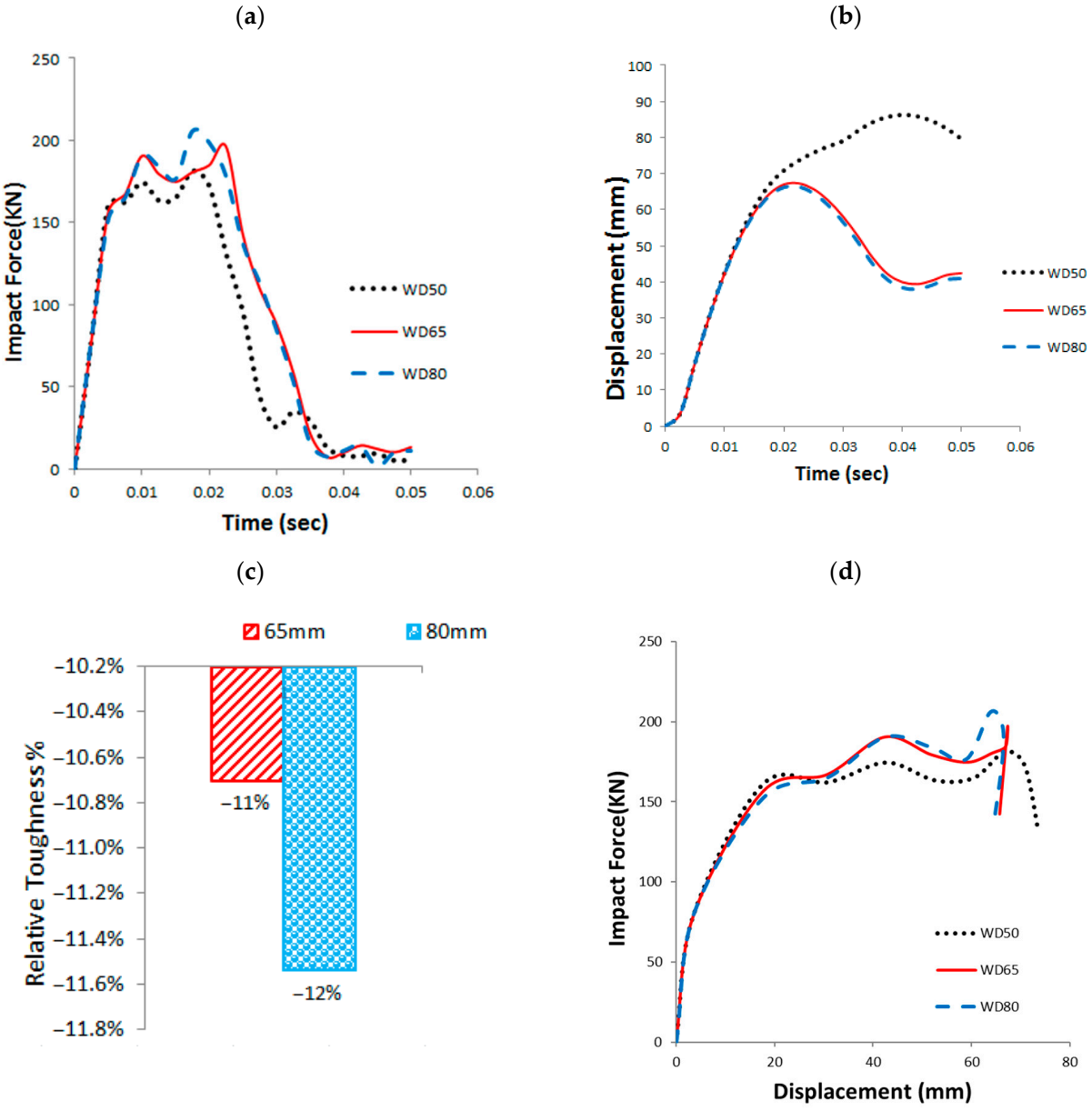

Figure 23. The effect of the GFRP poles with different washer diameter (WD): (**a**) the impact force time history, (**b**) the pole deflection time history, (**c**) normalized pole toughness of the studied cases with different washer diameter (WD), and (**d**) impact force—displacement curves of the GFRP poles having different washer diameters (mm).

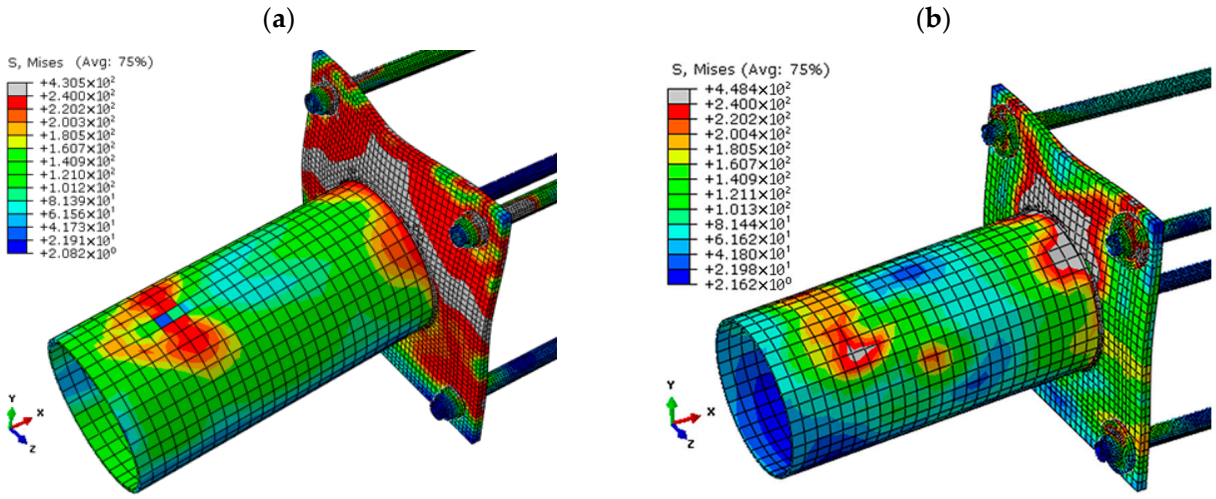

Figure 24. The von Mises stress distribution of the base plate and base sleeve: (**a**) 50 mm and (**b**) 80 mm.

The parametric analysis conducted in this study provides valuable insights into the influence of geometric and material parameters on the dynamic performance of GFRP lighting poles under vehicular impact. The results confirm that base geometry plays a more significant role in energy dissipation and failure response than material strength alone. Increased stiffness from thicker walls or base plates reduces energy absorption by limiting deformation. In contrast, more flexible designs promote better energy dissipation and delayed failure. Anchor bolt configurations affect load transfer, but material upgrades (e.g., S235 to S355 steel) offer minimal performance gains. Enlarging cable holes improves energy absorption but introduces stress concentrations that may lead to local failure. These findings align with and expand upon previous studies, confirming that structural geometry and joint design are more critical to crashworthiness than material strength alone. this work offers a dynamic, energy-based perspective that can be directly used in developing safer roadside infrastructure.

4. Conclusions

This research presents a comprehensive numerical investigation into the nonlinear dynamic behavior of GFRP lighting poles subjected to vehicular impact loads. A validated finite element (FE) model was developed and employed to conduct parametric study. The study revealed that energy absorption in GFRP–steel hybrid systems is predominantly governed by geometric flexibility and deformation capacity rather than material strength alone. While increasing the steel grade (e.g., from S235 to S355) marginally improved normalized toughness, major gains in energy dissipation were achieved through reductions in wall thickness, base plate stiffness, and sleeve height—parameters that control local plasticity and collapse behavior. These findings underscore the critical role of structural configuration in enhancing the dynamic crash performance of composite systems. Based on the numerical findings, the following conclusions were drawn:

- Increasing the GFRP pole wall thickness from 6 mm to 12 mm resulted in a 76% reduction in normalized toughness, indicating a shift to faster collapse with minimal deflection, thereby enhancing passenger safety.
- Increasing the base plate dimensions from 450 mm to 600 mm led to a 35% decrease in normalized toughness and promoted sleeve failure before base plate yielding, facilitating more efficient energy dissipation.

- Increasing the base plate thickness from 10 mm to 30 mm caused a 26% reduction in normalized pole toughness. Thinner plates allowed for more plastic deformation and better energy absorption, while thicker plates led to stiffer behavior and quicker collapse.
- Upgrading the base plate steel grade from S235 to S355 increased normalized toughness by 11%, though this also reduced deformation and shifted failure from the plate to the sleeve-weld region.
- Increasing the base sleeve height from 200 mm to 500 mm led to a 13% reduction in normalized toughness and quicker structural failure. In contrast, increasing the sleeve thickness from 2 mm to 8 mm caused only a 7% reduction in toughness, with thicknesses above 3 mm showing minimal additional benefit.
- Enlarging the electric cable hole diameter from 60 mm to 200 mm increased normalized toughness by up to 36.5%, though it raised local stress concentrations and introduced risks of weld failure.
- Using eight anchor bolts instead of four increased the normalized toughness by 11% and minimized base plate deformation and rotation. However, increasing the anchor bolt diameter from 22 mm to 30 mm reduced normalized toughness by 32%, indicating that larger diameters reduce the pole's energy absorption capacity.
- Changing the material grade of the base sleeve and anchor bolts from S235 to S355 resulted in minimal changes in normalized toughness—approximately 1.1% and 8% reductions, respectively—demonstrating limited influence on global dynamic performance.
- Increasing the washer diameter from 50 mm to 80 mm led to a 12% reduction in normalized toughness, suggesting a trade-off between improved fixation and reduced energy absorption.

In conclusion, the study underscores the importance of optimizing base geometry over material enhancements for improving the crashworthiness of GFRP poles. Future work is recommended to explore alternative materials (e.g., aluminum or GFRP sleeves), various sleeve shapes, and different connection mechanisms—such as screw bolts or rivets—as alternatives to conventional welding. These investigations could further enhance the safety and performance of GFRP poles under real-world impact conditions.

Author Contributions: Conceptualization, M.T.N. and O.E.; methodology, M.T.N. and M.E.K.; software, M.E.K.; validation, A.E., I.T.A., and M.T.N.; formal analysis, M.E.K.; investigation, M.T.N. and I.T.A.; resources, M.T.N.; data curation, M.T.N. and M.E.K.; writing—original draft preparation, M.E.K.; writing—review and editing, A.E., O.E., and I.T.A.; visualization, A.E.; supervision, M.T.N. and O.E.; project administration, M.T.N. All authors have read and agreed to the published version of the manuscript.

Funding: This research received no external funding.

Data Availability Statement: Data available on request.

Acknowledgments: The authors would like to express their sincere gratitude to Prince Sultan University (PSU), Riyadh, Saudi Arabia, for the generous support and funding provided for this research.

Conflicts of Interest: The authors declare no conflict of interest.

References

1. Elmarakbi, A.; Fielding, M.N. New Design of Roadside Pole Structure: Crash Analysis of Different Longitudinal Tubes Using LS-DYNA. 2009. Available online: https://www.dynalook.com/conferences/european-conf-2009/B-VI-04.pdf (accessed on 1 April 2024).
2. Abdel-Nasser, Y.; Alrajhi, J.; Alardhi, M.; Alkhulaifi, K. Frontal Crash Simulation of Vehicles Against Lighting Columns in Kuwait Using FEM. *Int. J. Traffic Transp. Eng.* **2013**, *2013*, 101–105. [CrossRef]

3. Elmarakbi, A.M.; Sennah, K.M. Frontal impact finite element modeling to develop FRP energy absorbing pole structure. *Int. J. Automot. Technol.* **2006**, *7*, 555–564.
4. Arafa, I.T.; Elhosseiny, O.M.; Nawar, M.T. Damage assessment of perforated steel beams subjected to blast loading. *Structures* **2022**, *40*, 646–658. [CrossRef]
5. Elmarakbi, A.; Krznaric, V.; Sennah, K.; Altenhof, W.; Chapman, M. Crashworthiness of vehicle-to-pole collisions using a hybrid III three-year-old child dummy. *Int. J. Veh. Syst. Model. Test.* **2013**, *8*, 1. [CrossRef]
6. Reddy, T.J.; Rao, Y.V.D.; Narayanamurthy, V. Thin-walled structural configurations for enhanced crashworthiness. *Int. J. Crashworth.* **2018**, *23*, 57–73. [CrossRef]
7. Samtani, N.C.; Kulicki, J.M. Reliability Evaluation of Concrete Cover for Buried Structures from Chloride-Induced Corrosion Perspective. *J. Bridge Eng.* **2020**, *25*, 4020049. [CrossRef]
8. Višnja, A.P.; Lakušić, T. Safety of roadside columns in case of vehicle impact The safety of roadside columns in the event of vehicle impact. *Građevinar* **2012**, *64*, 305–313.
9. Williams, G.L.; Kennedy, J.V.; Carroll, J.A.; Beesley, R. *The Use of Passively Safe Signposts and Lighting Columns*; TRL: Wokingham, UK, 2008.
10. EL-Fiky, A.M.; Awad, Y.A.; Elhegazy, H.M.; Hasan, M.G.; Abdel-Latif, I.; Ebid, A.M.; Khalaf, M.A. FRP Poles: A State-of-the-Art-Review of Manufacturing, Testing, and Modeling. *Buildings* **2022**, *12*, 1085. [CrossRef]
11. Stankevich, S.; Bulderberga, O.; Tarasovs, S.; Zeleniakiene, D.; Omastova, M.; Aniskevich, A. Electrical conductivity of glass fiber-reinforced plastic with nanomodified matrix for damage diagnostic. *Materials* **2021**, *14*, 4485. [CrossRef]
12. Tripathi, S.; Gupta, S.; Kumar, V.; Tiwari, P. Hybrid Utility Poles and their application in Power System: Refinement in Construction and Design of Conventional Utility Pole. In Proceedings of the International Conference on Electrical and Electronics Engineering, ICE3 2020, Gorakhpur, India, 14–15 February 2020. [CrossRef]
13. Metiche, S.; Masmoudi, R. Full-scale flexural testing on fiber-reinforced polymer (FRP) poles. *Open Civ. Eng. J.* **2007**, *1*, 37–50.
14. Metiche, S.; Masmoudi, R. Analysis and design procedures for the flexural behavior of glass fiber-reinforced polymer composite poles. *J. Compos. Mater.* **2013**, *47*, 207–229. [CrossRef]
15. Son, J.K.; Fam, A. Finite element modeling of hollow and concrete-filled fiber composite tubes in flexure: Model development, verification and investigation of tube parameters. *Eng. Struct.* **2008**, *30*, 2656–2666. [CrossRef]
16. Bondok, D.H.; Salim, H.A. Numerical Modeling of Conventional Steel Stud Walls' Static Resistance for Blast Response Predictions. *J. Struct. Eng.* **2014**, *140*. [CrossRef]
17. Nawar, M.T.; Arafa, I.T.; Elhosseiny, O.M.; El-Zohairy, A. Full static resistance of castellated steel beams with hexagonal web openings for blast response predictions. *Eng. Struct.* **2021**, *245*, 112844. [CrossRef]
18. Desai, N.; Yuan, R. Investigation of bending/buckling characteristics for FRP composite poles. In Proceedings of the Earth and Space 2006—Proceedings of the 10th Biennial International Conference on Engineering, Construction, and Operations in Challenging Environments, League City/Houston, TX, USA, 5–8 March 2006. [CrossRef]
19. Ibrahim, S.; Polyzois, D. Ovalization analysis of fiber-reinforced plastic poles. *Compos. Struct.* **1999**, *45*, 7–12. [CrossRef]
20. Polyzois, D.; Ibrahim, S.; Raftoyiannis, I.G. Performance of fiber-reinforced plastic tapered poles under lateral loading. *J. Compos. Mater.* **1999**, *33*, 941–960. [CrossRef]
21. Urgessa, G.; Mohamadi, S. Structural Assessment of Fiber-reinforced Polymer Composite Electric Poles. *Procedia Eng.* **2016**, *145*, 707–714. [CrossRef]
22. Fam, A.; Kim, Y.J.; Son, J.K. A numerical investigation into the response of free end tubular composite poles subjected to axial and lateral loads. *Thin-Walled Struct.* **2010**, *48*, 650–659. [CrossRef]
23. Gao, H.; Sun, Y.; Jian, J.; Dong, Y.; Liu, H. Study on mechanical properties and application in communication pole line engineering of glass fiber reinforced polyurethane composites (GFRP). *Case Stud. Constr. Mater.* **2023**, *18*, e01942. [CrossRef]
24. Awad, Y.A.; El-Fiky, A.M.; Elhegazy, H.M.; Hasan, M.G.; Yousef, I.A.; Ebid, A.M.; Khalaf, M.A. Behavior of Centrifuged GFRP Poles Under Lateral Deflection. *Civ. Eng. J.* **2023**, *9*, 1389–1401. [CrossRef]
25. Nawar, M.T.; Kaka, M.E.; El-Zohairy, A.; Elhosseiny, O.; Arafa, I.T. Effect of Supporting Base System on the Flexural Behavior and Toughness of the Lighting GFRP Poles. *Sustainability* **2022**, *14*, 12614. [CrossRef]
26. Noh, J.; Ghadimi, B.; Russo, S.; Rosano, M. Assessment of FRP pultruded elements under static and dynamic loads. *Compos. Struct.* **2018**, *202*, 17–28. [CrossRef]
27. Polyzois, D.; Raftoyiannis, I.G.; Philopulos, D. An experimental survey of the static and dynamic behavior of jointed composite GFRP tapered poles. *Mech. Adv. Mater. Struct.* **2007**, *14*, 203–212. [CrossRef]
28. Caracoglia, L.; Velazquez, A. Experimental comparison of the dynamic performance for steel, aluminum and glass-fiber-reinforced-polymer light poles. *Eng. Struct.* **2008**, *30*, 1113–1123. [CrossRef]
29. Zhang, Y.; Pan, R.; Xiao, F. Numerical research on impact performance of bridge columns with aluminum foam protection devices. *Int. J. Distrib. Sens. Netw.* **2020**, *16*, 1550147720974538. [CrossRef]

30. Al-Thairy, H.; Wang, Y.C. Simplified FE vehicle model for assessing the vulnerability of axially compressed steel columns against vehicle frontal impact. *J. Constr. Steel Res.* **2014**, *102*, 190–203. [CrossRef]
31. Kang, H.; Kim, J. Response of a steel column-footing connection subjected to vehicle impact. *Struct. Eng. Mech.* **2017**, *63*, 125–136. [CrossRef]
32. Wang, J.; GangaRao, H.; Liang, R.; Liu, W. Experimental and Analytical Responses of Hollow and Concrete-Filled GFRP Tube Columns under Impact. *J. Compos. Constr.* **2017**, *21*, 04017013. [CrossRef]